The bottom mixed layer depth (BMLD) as an indicator of subsurface chlorophyll-a distribution

Arianna Zampollo[1,*], Thomas Cornulier[1], Rory O'Hara Murray[2], Jacqueline Fiona Tweddle[1], James Dunning[1], Beth E. Scott[1]

[1] School of Biological Sciences, University of Aberdeen, Aberdeen, AB24 2TZ, UK

[2] Marine Scotland Science, Aberdeen, AB11 9DB, UK

Correspondence to: Arianna Zampollo (zampolloarianna@gmail.com)

Abstract

Primary production dynamics are strongly associated with vertical density profiles in shelf waters. Variations in the vertical structure of the pycnocline in stratified shelf waters are likely to affect nutrient fluxes, hence the vertical distribution and production rate of phytoplankton. To understand the effects of physical changes on primary production, identifying the linkage between water column density and chlorophyll-a (Chl-a) profiles is essential. Here, the vertical distributions of density features describing three different portions of the pycnocline (the top, central aspects, and the end) were compared to the vertical distribution of Chl-a to provide auxiliary variables to estimate Chl-a in shelf waters. The proximity of density features with deep Chl-a maximum (DCM) was tested using Spearman correlation, linear regression, and a major axis regression over 15 years in a shelf-sea region (the northern North Sea) that exhibits stratified water columns. Out of 1237 observations, 78% reported DCM above the bottom mixed layer depth (BMLD: depth between the end of the pycnocline and the below mixed layer) with an average distance of 2.74 ± 5.21 m from each other. BMLD acts as a vertical boundary above which subsurface Chl-a maxima are mostly found in shelf seas (depth ≤ 115 m). Overall, DCMs correlated to the halfway depth of the pycnocline (ρ_S = 0.56), which combined with BMLD, were better predictors of the locations of DCMs than surface mixed layer indicators and the maximum squared buoyancy frequency. These results suggest a significant contribution of deep mixing processes in defining the vertical distribution of subsurface production in stratified waters and indicate BMLD as a potential indicator of the Chl-a spatiotemporal variability in shelf seas. An analytical approach integrating the threshold and the maximum angle method is proposed to extrapolate BMLD, the surface mixed layer and DCM from *in situ* vertical samples.

Keywords

buoyancy frequency, deep mixing, deep Chl-a maximum (DCM), mixed layer depth (MLD), halfway pycnocline depth (HPD).

1. Introduction

As we begin to manage our oceans and shelf seas for more complex simultaneous uses, such as renewable energy developments, fishing and marine protected areas, it is becoming increasingly important to understand the details of primary productivity at fine spatial scales. Besides very shallow waters, the vast majority of phytoplankton production in continental shelf waters generally occurs under stratified conditions, where the pycnocline provides a stable habitat for phytoplankton growth in the lower euphotic zone. The seasonal heating-cooling cycle of the water column regulates the stratification in temperate shelf waters, where the intensified solar radiation in spring-summer increases the difference of temperature and salinity between surface and deep waters and prompts the formation of a pycnocline dividing surface from deep mixed waters. Once the stratification is set in spring-summer, turbulent mixing represents the main source of new nutrients into the pycnocline during prolonged stratified conditions. Climate change (Holt et al., 2016, 2018) and the introduction of numerous man-made infrastructures (e.g. offshore wind farms, Dorrell et al., 2022) are expected to alter the balance between mixing and stratification in shelf regions, affecting the vertical exchange of nutrients between deep and surface waters (below and above the pycnocline). Anomalies such as circulation slow-down, sea-level rise, bottom and surface temperature, wind speed and wave height have largely been described as a consequence of climate change in the last two decades (e.g. Orihuela-Pinto et al., 2022; Taboada and Anadón, 2012; Bonaduce et al., 2019), while the consequences of these physical changes on the biological processes are still partially understood (Lozier et al., 2011; Somavilla et al., 2017).

1.1 Subsurface chlorophyll-a maxima

Many of the uncertainties related to estimating primary production abundance are related to the difficulties in retrieving correct concentrations throughout the whole water column. Contrary to the detection of surface blooms by satellite sensors, subsurface chlorophyll-a maxima (SCM) are often more difficult to measure. SCMs represent significant features in plankton systems (Cullen, 2015), they define where most of the bottom-up processes take place, they can persist in separate vertical layers and encompass more than 50% of the entire water column production (Weston et al., 2005; Takahashi and Hori, 1984). In the North Sea, the summertime (May-August) subsurface production contributes to 20-50% of the annual production and sustains the food chain in continental shelf waters during prolonged stratified conditions (Hickman et al., 2012; Richardson and Pedersen, 1998; Weston et al., 2005). Several studies linked the vertical distribution of maxima chlorophyll-a (DCMs) to deep mixing processes (e.g. Brown et al., 2015; Richardson and Pedersen, 1998; Sharples et al., 2006) and identified the occurrence of deep assemblages in the proximity of the pycnocline in shelf seas (e.g.

Costa et al., 2020; Durán-Campos et al., 2019; Ross and Sharples, 2007; Sharples et al., 2001). DCMs have been identified close to the base of the pycnocline in regions of strong tidal mixing at Georges Bank in August (Holligan et al., 1984) and at the western English Channel (Sharples et al., 2001). However, despite the clear linkage between SCM and subsurface physical processes in shelf seas, only surface mixing processes have been used to investigate the global variations of primary production (Somavilla et al., 2017; Steinacher et al., 2010) making the surface mixed layer depth (MLD) one of the main indicator for the variations of density structures and marine primary production. However, shelf ecosystems are equally driven by physical processes occurring above and below the pycnocline (Wihsgott et al., 2019), making the identification of the upper and below limits of the pycnocline essential to understand the processes defining the primary production in shelf waters.

1.2 The surface mixed layer depth (MLD)

MLD has been largely considered as a central variable for understanding phytoplankton dynamics (Sverdrup, 1953), especially in oceanic sites, where several studies have investigated the association of MLD with Chl-a vertical distribution (Behrenfeld, 2010; Carranza et al., 2018; Diehl, 2002; Diehl et al., 2002; Gradone et al., 2020), phytoplankton bloom events (Behrenfeld, 2010; Chiswell, 2011; D'Ortenzio et al., 2014; Prend et al., 2019; Ryan-Keogh and Thomalla, 2020, Sverdrup, 1953), and the effects of climate change (Somavilla et al., 2017). The nutricline depth exhibits positive correlations with the upper mixed layer depth (Ducklow et al., 2007; Gradone et al., 2020; Holligan et al., 1984; Prézelin et al., 2000, 2004; Ryan-Keogh and Thomalla, 2020; Yentsch, 1974, 1980), and it has been generally associated with surface spring blooms or windstorm events (Carranza et al., 2018; Carvalho et al., 2017). However, the effects of MLD and climate's variations on primary production are still an unsolved question (Lozier et al., 2011; Somavilla et al., 2017). The need for a much more detailed understanding of the linkage between primary production, pycnocline characteristics and deep turbulent processes (below the pycnocline) is therefore a key area of research, especially in highly productive but spatially heterogeneous areas such as shelf waters and shallow seas.

The methods for identifying MLDs vary among marine environments, hydrodynamic regimes, or the spatial resolution of vertical profiles (Courtois et al., 2017; Lorbacher et al., 2006), because making use of a single method is difficult for spatiotemporally heterogeneous regions. MLDs are typically defined as the depth at which the density exceeds a specific value (threshold method), however this method presents issues in specific hydrodynamic conditions, such as over estimating MLD in regions with deep convection (e.g. subpolar oceans) (Courtois et al., 2017), or misidentifying water columns with a newly established shallow MLD over previous periods of stratification (Somavilla et al., 2017). Several sensitivity tests and comparisons have been conducted in oceanic waters (González-Pola et al., 2007; Holte and Talley, 2009; Courtois et al., 2017), however, there are no standard methods for MLD identification neither in shelf nor oceanic waters.

1.3 A new way forward: the bottom mixed layer depth (BMLD) as an indicator of deep Chl-a maxima (DCMs) in shelf waters

In temperate shelf waters after spring blooms, phytoplankton adapt to grow at the subsurface under low light and nutrient conditions where new primary production is sustained by upward nutrient fluxes from the mixed layer below the pycnocline (bottom mixed layer, BML) (Pingree and Griffiths, 1977; Wihsgott et al., 2019). Several studies reported the vertical distribution of SCMs close to the base of the pycnocline (e.g. Costa et al., 2020; Durán-Campos et al., 2019), especially in stratified waters affected by tidal currents in the proximity of shelf banks. As an example, spring tides have been shown to trigger a hydraulic jump on the edge of the Jones Bank (Celtic Sea, UK) that is sufficient to increase the mixing at the base of the pycnocline and inject it with new nutrients (Palmer et al., 2013). The BML is crucial in supporting subsurface primary production in resource limited environments where turbulent mixing in the proximity of the thermocline introduces new nutrients in surface waters and removes phytoplankton from the SCM into deep waters (Western English Channel, Sharples et al., 2001). The upward transfer of nutrients and downward fluxes of phytoplankton occurring at the base of the pycnocline advocates this depth as a central location of carbon fluxes in temperate shelf waters (Sharples et al., 2001), making the upper limit of the bottom mixed layer in the proximity of the base of the pycnocline (hereafter called bottom mixed layer depth, BMLD) a key variable for estimating productivity. In the literature, BMLD has been identified as the depth where density changes -0.02 kg m^{-3} relative to the closest value to the seabed (Sharples et al., 2001; Wihsgott et al., 2019; Poulton et al., 2022; Hopkins et al., 2021) or by 0.01-0.1 °C above the near bed temperature (Palmer et al., 2013; Pingree and Griffiths, 1977). In this study:

- We proposed the adaptation of existing methods (threshold and maximum angle methods from Chu and Fan (2011)) into a new algorithm able to process different vertical distributions of high-resolution (1 m) density profiles (characterized by split pycnoclines) to identify i) the surface mixed layer (MLD) and ii) the bottom mixed layer depth (BMLD) in stratified waters.
- The depth-integrated Chl-a was compared among the sections above and below stratification features (MLD, halfway pycnocline depth, BMLD, and maximum squared buoyancy frequency) in shelf waters (20-120 m) using 15 years of repeated surveys covering a mosaic of habitats types:

seasonally stratified waters, permanently mixed waters, regions of freshwater inputs and strong tidal mixing (van Leeuwen et al., 2015). DCMs were hypothesized to distribute at the same depth of stratification structures to test where summertime subsurface Chl-a distribute more frequently in regard to the pycnocline (e.g. DCMs at the most stratified layer identified by Max N^2 or at the base of the pycnocline).

- Further scrutiny was applied to BMLD to investigate to which extent it can inform on the vertical distribution of DCMs in temperate, stratified, shelf waters during summer, regardless of any phytoplankton dynamic (cell's light history regulating photoacclimation) or physical conditions of the water column (e.g. stability).

2. Methods

2.1 Oceanographic data

In situ summertime measurements of temperature, salinity, and Chl-a were collected from a towed, undulating, and a vertical CTD-fluorometer in the North Sea off the East coast of Scotland, UK, within the Firth of Forth (FoF) and Tay region for over 15 years (from 2000 to 2014) (Figure 1). A total of 1273 profiles from both types of sampling were extracted from April to August (April=3, May=51, June=1115, July=66, August=38). 426 profiles from the sea surface to the seabed (vertical resolution equals to 1 decibar) were collected at fixed stations from 12 oceanographic campaigns carried out by Marine Scotland Science on board of the fisheries research vessels *Scotia* and *Alba na Mara* (www.gov.scot/marine-and-fisheries). Water samples were collected during each cast for calibration of the *in situ* sensor data. The undulating CTD-fluorometer sampled the water column in June 2003 and July 2014 with a continuous vertical and horizontal oscillation of the instrument throughout the water column from 2-5 m below the sea surface to 5 m from the seabed. The continuous profiles obtained from undulating CTD-fluorometer were converted into 847 single profiles of the water columns. Data were sampled at 1 second intervals, resulting in a vertical resolution comprising between 0.5 and 1 m, in water depths from 25 m to 115 m. Further information about the oceanographic cruise in June 2003 is described by Scott et al. (2010), whose method was applied in the cruise in July 2014.

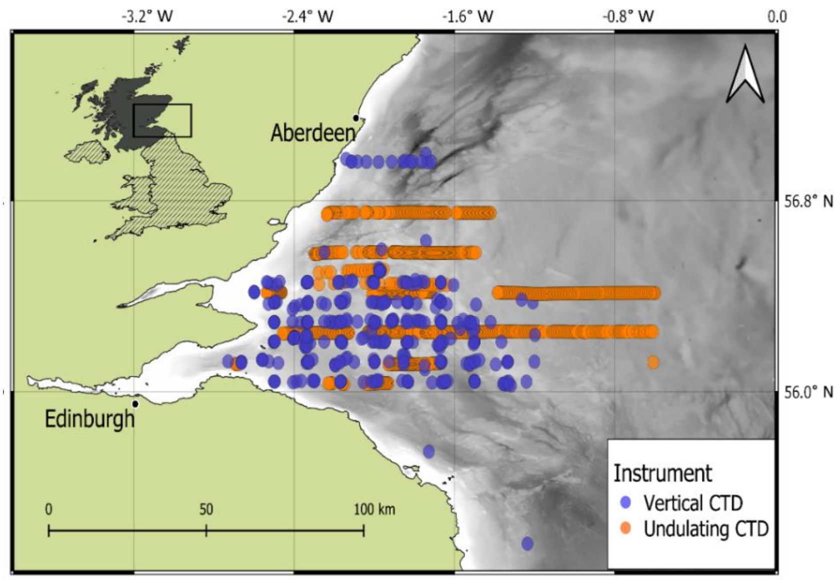

Figure 1: study area with the in situ surveys measured by a vertical CTD (blue dots) and an undulating CTD (orange dots). Land (green) and bathymetry (grey colour ramp) are pictured (EMODnet, 2018).

2.2 Standardized density profiles

Since the proposed algorithm works with profiles at high vertical resolution (1 m), the *in situ* casts must be standardized throughout the water column. Density (ρ) (kg m^{-3}) observations taken every 0.5 to 1 m from undulating CTD-fluorometer were converted into measurements over regular depth intervals by smoothing and interpolating. This was achieved by fitting a generalized additive model (GAM) (Hastie and Tibshirani, 1990) using an adaptive spline with ρ as a function of depth. The obtained smooth function for each profile was used to interpolate ρ at regular 1 m depth intervals. In order to maintain the same shape and values in each profile, the fitted curves at 1 m intervals were visually checked by plotting the estimated and real profiles to identify possible errors visually. 4.16% of the shapes (n=53) were manually corrected by changing the number of knots in the GAM, which ranged from 75% to 90% of the number of observations occurring within each profile. An example is given in Figure A2 in Appendix A. The analyses were run in R (R Core Team, 2018) using the *mgcv* package.

2.3 MLD and BMLD detection

Definition of MLD and BMLD

In stratified shelf waters, the layers above and below the pycnocline are mixed vertical region where the density gradient is significantly different from the pycnocline. The upper mixed layer depth (MLD) and the bottom mixed layer depth (BMLD) are both the transition regions between mixed waters and the pycnocline (Figure 2). The most common threshold methods (see Section 2.4) identify MLD and BMLD based on the principle that the mixed layer at the surface has a density's variance close to zero, which separates from the pycnocline, exhibiting a larger density gradient. The above assumptions may not always hold, especially when the upper mixed layer is heterogeneous with nested sub-structures such as small re-stratification at the surface, or when the pycnocline can include a thin mixed layer (Figure A1 a, e, f in Appendix A) or presents different density gradients (stratified layers) within it (Figure A1 b and c). Such density conditions are difficult to isolate with the available methods.

In the proposed algorithm, the detection of MLD does not assume only that the upper mixed layer has a density gradient close to zero up to the top of the pycnocline, and it firstly identifies MLD (and BMLD) regardless any *a priori* threshold (Chu and Fan, 2019, 2011; Holte and Talley, 2009). Two approaches, the angle's method from Chu and Fan (2011) and K-means clustering (Lloyd, 1982), are used to analyse the vertical distribution of density ρ by comparing the observations to each other in the same profile instead of applying an absolute threshold to all profiles. The algorithm distinguishes in the water column three layers having similar density values (the upper mixed layer, pycnocline and lower mixed layer) (Figure 2). The MLD represents the shallowest depth up to which the difference of density between adjacent points $\Delta\rho$ is small and similar from the surface. The BMLD is the first depth below the pycnocline from which $\Delta\rho$ is small and similar down to the seabed. This type of detection based on the density shape allows the identification for unconventional density vertical distribution (Figure A1 in Appendix A) in stratified waters. It is important to notice that this method does not determine whether the water column is stratified, and it can be applied to profiles exhibiting a pycnocline described by high-resolution, equally distant observations.

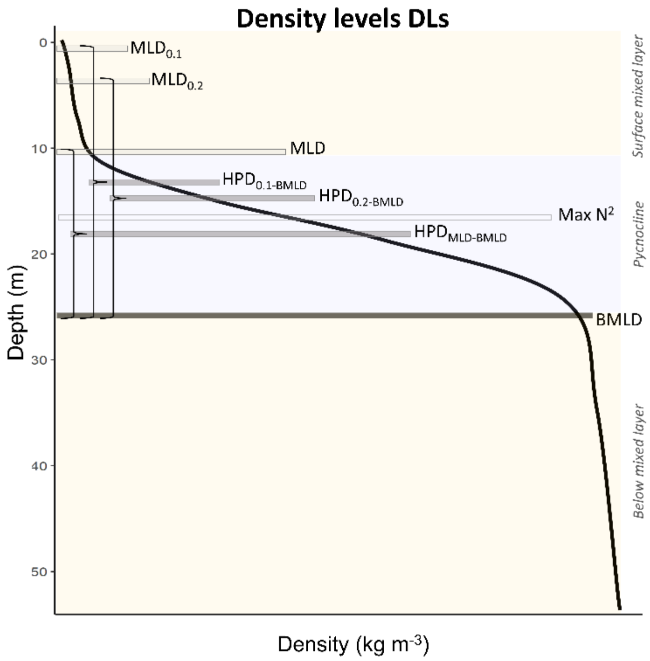

Figure 2: a generic density profile whose limits of the surface and below mixed layers (yellow rectangles) and pycnocline (grey rectangle) are displayed by density levels (DLs). The curly brackets define the halfway depths (HPDs) between MLD's indicators and BMLD.

Method to extract MLD and BMLD

The algorithm was developed in R (R Core Team, 2018) (available at https://github.com/azampollo/BMLD) and implements i) an adaptation of the maximum angle method (Chu and Fan, 2011) and ii) a cluster analysis on the density difference between two consecutive points ($\Delta\rho_z = |\rho_z - \rho_{z+1}|$). The method is designed to work with equal, high-resolution (1 m), intervals of density values (z) collected in stratified shelf waters, with a pycnocline detailed by > 5 values, and BMLD distributed within the first 90% of the observations from the surface to the deepest point (close to the seabed). The reason why the method is sensitive to the number of points within the pycnocline, before MLD and after BMLD, is due to the analyses included in the algorithm depending on at least two observations before and after each mixed layer depth.

The first steps of the algorithm follow the method by Chu and Fan (2011) where the depth exhibiting the maximum angle (φ) between two vectors (V1 and V2) referring to density conditions above and below it is selected as the mixed layer depth. At each observation (z) of the density profile, the method calculates the angle φ from the intersection of V1 and V2, each one fitted using a linear regression model that accounts for the vertical distribution of the density values above (for V1) or below (for V2) *z*. At each *z* of the density profile, a unique V1 (blue line in Figure 3) is fitted using *z* and 2 points (2δ) above it, and a unique V2 (red line in Figure 3) is fitted using *z* and 2 points below it. The angle φ resulting from the intersection of the two lines is measured in degrees using Eq. S1 reported in

Supplementary material. Although Chu and Fan (2011) suggested to identify MLD by measuring the tangent of the angle between V1 and V2, we encountered some issues identifying BMLD in those profiles where φ was bigger than 90 degrees, and where density slightly decreased below the pycnocline (Figure A1 d in Appendix A). At this point, an angle φ is associated with each observation in the density profile. Since the identifications of MLD and BMLD are both based on the ranking of φ, the selection of either one or the other requires splitting the density profile into "surface" (Split1) and "deep" (Split2) observations to avoid any misidentification and interchange between mixed layer depths. *Split1* includes the density values from the surface (z_1) to two measurement intervals (2δ) above BMLD (Figure 3 a), while *Split2* extends from 2δ above the halfway depth in ρ range ($0.5\Delta\rho = ((\rho_{\max} - \rho_{\min})/2) - 2$) to the ninetieth portion of the profile from the surface to the seabed ($z_{0.9\Delta\rho}$ = 90% of ${}_1^n z$) (Figure 3 b). The bottom limit of Split2 was defined at $z_{0.9\Delta\rho}$ following Chu and Fan (2011) to reduce the number of observations close to the seabed. However, the analyses can be extended up to the end of the profile (see https://github.com/azampollo/BMLD).

After the selection of the largest angles as potential MLD and BMLD, a further K-Mean cluster analysis (Lloyd, 1982) was used to identify the mixed and stratified layers based on the density difference between two consecutive points ($\Delta\rho_z$). The cluster analysis satisfied the assumption that similar observations belong to either the mixed or stratified layers. MLD and BMLD were hence selected above the candidates whether the observations above and below them belonged to the same cluster. More details regarding the decisional tree of the algorithm are reported in the Supplementary materials. Adding the conditions controlling for a similar density gradient above MLD and below BMLD decisively improved the selection of pycnocline's limits in pycnocline fractured in chunks. Moreover, several trials reported that the exclusive use of the maximum angle method would have biased the selection due to local variation and instability conditions of the water column (Figure A1 b, c, e, f in Appendix A).

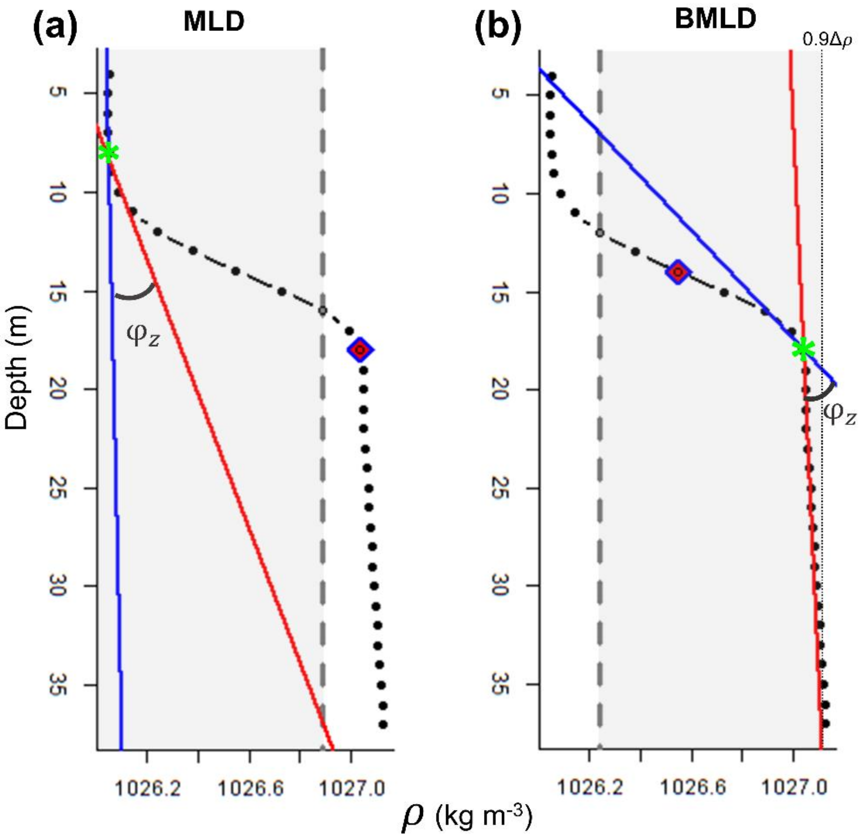

Figure 3: plots of a density profile reporting the attributes calculated by the algorithm: grey region includes the observations (z) (black dots) used to identify (a) MLD within Split1 and (b) BMLD within Split2. Split1 extends from the surface to 2δ above BMLD (purple rhombus), and Split2 from 2δ above half of the profile's density range (0.5Δρ, purple rhombus) to 0.9Δρ. The solid blue and red lines refer to the vectors V1 and V2, whose intersection defines the angle φ_z selected as MLD and BMLD (green stars).

Performance of the algorithm

The algorithm was validated by manually checking the estimated MLD and BMLD in each profile, which were considered wrongly identified when falling into the pycnocline. Since most of the errors located the mixed layer depths clearly at the centre of the pycnocline having thin layers of re-stratification (> 4 observations) (Figure A1 b, c, e, f in Appendix A), the identifications were considered correct when they appeared i) on top of a bottom mixed layer (in the BML) and ii) on top of a large density gradient (pycnocline) separating surface to deep waters. Major errors in identifying MLD (6.76% of the profiles) and BMLD (4.32%) occurred in density profiles with a smooth transition from the mixed layer to the pycnocline, hence reporting a high number of observations at the mixed layer depths (e.g. Figure A1 a-c). It is important to highlight the sensitivity of this method to the difference in density ($\Delta\rho$) at MLD and BMLD (a large $\Delta\rho$ is preferred), and to the sampling frequency at the transition regions between mixed waters and the pycnocline. The algorithm did not correctly identify MLD in profiles with a shallow pycnocline (no upper mixed layer) that comprised two different gradients (Figure A1 c). In this case, the cluster analysis split $\Delta\rho$ within the pycnocline into two groups, although they belong to the same pycnocline. Other errors were related to profiles having a pycnocline split into two parts by a thin mixed layer having > 4 observations (Figure A1 e). Overall, the identification of BMLD performed better than MLD's, although it could not deal with profiles having less than 4 observations throughout the pycnocline (thickness of the pycnocline < 4 m). This condition occurred due to the location of the *Split2* (which is necessary to distinguish BMLD's from MLD's selection) i) at depths above MLD (misidentifying MLD as BMLD) or ii) too close to BMLD (lacking observations to properly fit V1). The algorithm always correctly selected BMLD in profiles with a temporary overturn in the density profile (Figure A1 d).

2.4 Common methods identifying Density Levels (DLs)

The depths detailing the density structure in the water column are defined here as density levels (DLs). Among the multiple indicators of mixed layers that associate with Chl-a vertical distribution, the surface mixed layer depth, the halfway pycnocline depth (HPD) and the maximum squared buoyancy depth were compared to the proposed algorithm's identifications (MLD and BMLD).

The MLD and BMLD are typically defined in the literature as the depth at which the density exceeds a specific value (threshold method). The threshold is typically selected among a range of values previously tested in the literature (from 0.0025 to 0.125 kg m^{-3}) (summarized in Thomson and Fine, 2003; Montégut et al., 2004; Lorbacher et al., 2006; Holte and Talley, 2009) and measured as the difference ($\Delta\rho_z = |\rho_z - \rho_{ref}|$) between a certain sampling depth (z) and a reference density value (ρ_{ref}), which can be the density at the surface, at a specific depth (e.g. 10 m), or a consecutive point (e.g. z-1). In this study, two density thresholds (0.01 and 0.02 kg m^{-3}) have been measured as the difference between two consecutive points in the profile ($\Delta\rho_z = |\rho_z - \rho_{z+1}|$) and named $MLD_{0.01}$ and $MLD_{0.02}$.

Since previous studies identified subsurface Chl-a in the proximity of the centre of the pycnocline (hereafter called halfway pycnocline depth – HPD), we investigated the relationship between DCM and three different HPDs measured as the halfway depth between the bottom mixed layer depth (BMLD) and $MLD_{0.01}$, $MLD_{0.02}$ and MLD: $HPD_{0.01\text{-}BMLD}$, $HPD_{0.02\text{-}BMLD}$, and $HPD_{MLD\text{-}BMLD}$ (Table 1, Figure 2).

Moreover, several studies reported positive correlation between the maximum squared buoyancy frequency (Max N^2) and DCM at oceanic sites (e.g. Martin et al., 2010; Schofield et al., 2015; Carvalho et al., 2017; Courtois et al., 2017; Baetge et al., 2020) and shelf waters (Lips et al., 2010; Zhang et al., 2016). Therefore, the depth of Max N^2 has been selected from N^2 profiles using *gsw* package in R (R Core Team, 2018) following the most recent version of the Gibbs equation of state for seawater in TEOS-10 systems. The magnitude of N^2 quantifies the stability of the water column and pinpoints the stratified layers where the energy required to exchange water parcels in the vertical direction is maximum (Boehrer and Schultze, 2009).

Table 1: list of abbreviations.

Abbreviation	***Description***
BMLD	*Bottom mixed layer depth* (m)
Chl-a	*Chlorophyll-a* (mg m^{-3})
DCM	*Deep chlorophyll-a maximum (m)*
DL	General abbreviation for a *density level* (e.g. MLD, BMLD, HPD, or Max N^2) (m)
HPD	*Halfway pycnocline depth*, or centre of the pycnocline (m)
Max N^2	maximum squared buoyancy frequency (N^2) (m)
MLD	*Mixed layer depth,* or top of the pycnocline (m)
SCM	*Subsurface chlorophyll-a maximum* (mg m^{-3})

2.5 Subsurface Chlorophyll-a parameters

Deep Chl-a maxima (DCMs) were defined as the deepest maximum inflection point in the Chl-a profile with 1 m sampling frequency (Carvalho et al., 2017; Zhao et al., 2019). Here, the inflection point is defined as the depth exhibiting a high concentration of Chl-a and a large change in Chl-a values throughout the profile. The DCM was investigated using the adapted Chu and Fan (2011) method identifying for φ described in Section 2.3. The angle φ was measured at each depth of the Chl-a profile, and the largest angle with the greatest Chl-a concentration was selected as DCM. The automated identification of DCM was checked manually with a visual inspection of each profile. The method is available under the function *maxChla.R* (R Core Team, 2018) at https://github.com/azampollo/BMLD.

The depth-integrated Chl-a were measured using trapezoidal integration (Walsby, 1997) throughout the water column.

2.6 Evaluating the association of density levels with subsurface Chl-a

The proximity of each density level (DL) to subsurface aggregations of Chl-a was evaluated by comparing their coincidence with DCM (e.g. DCM = BMLD) and their strength in predicting DCM. In this study, we investigate the use of the surface mixed layer depth ($MLD_{0.01}$, $MLD_{0.02}$, MLD), the maximum squared buoyancy depth (Max N^2), halfway pycnocline and bottom mixed layer depths

($HPD_{0.01\text{-}BMLD}$, $HPD_{0.02\text{-}BMLD}$, $HPD_{MLD\text{-}BMLD}$, and BMLD) to derive i) the vertical distribution of Chl-a by using Spearman's rank correlation coefficient (ρ_S) and a major axis line fitting, and ii) the prediction of DCM from DL by performing a linear regression model. All three methods differently assess the correlation or prediction. The Spearman's coefficient (Eq. 1 in Table 2) assesses a monotonic linear relationship with values ranging between -1 and +1, which refer to a perfect negative or positive correlation between two variables. Besides the strength of the linear relationship defined by ρ_S, we focused on evaluating the linear relationship between DCM and each DL using 3 different linear models $y = \alpha + \beta x$: 1) α and β estimated by linear regression; 2) α and β estimated by major axis line fitting; and 3) the one-to-one linear regression with α and β fixed at 0 and 1 respectively. The one-to-one line hypothesizes that DCM and DL occur at the same depth. The major axis regression is largely used to investigate how one variable scales against another by assuming the departures from the fitted line in both directions (x and y) have equal importance (details in the review Warton et al., 2006). Therefore, the aim of the analysis is not to predict the y-variable, however evaluating whether the line-of-best-fit measured by the major axis correspond to the one-to-one line where any DL equals DCM. The coincidence of each DL and DCM was summarized by reporting the α and β coefficients, which are hypothesized to be intercept ~ 0 and slope ~ 1 when DCM occurs at the same depth of the DL in question.

Since the identification of drivers for subsurface Chl-a represents a useful tool for correctly assessing the abundance and the variations of primary production, we investigated the power of prediction of DCM from each DL by measuring the r-squared (R^2) from i) an ordinary least square to estimate parameters from the observations in a linear regression (Eq. 2 in Table 2), and ii) the one-to-one linear regression (which has been forced with the intercept through the origin and a slope equal to 1, Eq. 3 in Table 2). The equations used to calculate the coefficient of determination R^2 for the one-to-one (R_0^2) and empirical (R_{em}^2) linear regressions are summarized in Eq. 2 and Eq. 3 in Table 2.

Table 2: equations for estimating the bivariate line-fitting. Spearman's rank correlation coefficient (ρ_S), coefficient of determination R^2 for testing the one-to-one linear regression (R_0^2) (e.g. DCM ~ BMLD) and the empirical linear regression (R_{em}^2).

	Formula		**Purpose**
ρ_S	$\frac{\sigma_{xy}}{\sigma_x \sigma_y}$	Eq. 1	Estimate the strength of the relationship between x and y
R_{em}^2	$1 - \frac{SS_{RES}}{SS_{TOT}} = 1 - \frac{\sum_{i=1}^{n}(y_i - \hat{y}_i)^2}{\sum_{i=1}^{n}(y_i - \bar{y})^2}$	Eq. 2	Measure the variation in y that is explained by x in a linear regression

R_0^2	$1 - \frac{SS_{RES}}{SS_{TOT}} = 1 - \frac{\sum_{i=1}^{n}(y_i - x_i)^2}{\sum_{i=1}^{n}(y_i)^2}$	Eq. 3	Measure the variation in y that is explained by x in a one-to-one linear regression

Notation: σ_{xy} is the covariance of x and y, σ_x and σ_y are standard deviations, n is the number of observations of x and y, y_i is DMC_i, $\bar{y}$ is the average of DCMs, and x_i is the density layers related to DCM in each regression (e.g. DCM ~ BMLD). SS_{RES} is the residual sum of squares, SS_{TOT} is the total sum of squares.

In the empirical linear regression, R_{em}^2 was calculated using the typical equation with the residual sum of squares (SS_{RES}) as the square of the difference of y and $\hat{y}$ (estimated y from the model) (Eq. 1). In the one-to-one linear regression, the SS_{RES} in R_0^2 was adapted by replacing $\hat{y}$ with x (Eq. 3), since the values of x and y are assumed to be equal in the one-to-one line regression and the difference between them should be zero. The two R^2 differ also for the denominator SS_{TOT}, which is the sum of squares about the average of the explanatory variable in R_{em}^2 and the sum of squares of the DCM values since in R_0^2 the value of DCM and DL equals.

Since the SS_{TOT} adopted in the two equations is different, the proportion of explained DCMs' variance by each DL can be compared only within each linear regression rather than across the one-to-one and empirical regressions. Therefore, the power of prediction among DLs was discussed within each type of linear regression.

3. Results

The proposed hybrid method identifying for MLD and BMLD was applied to 1273 profiles exhibiting a pycnocline. The associations of the density levels ($MLD_{0.01}$, $MLD_{0.02}$, MLD, $HPD_{0.01\text{-}BMLD}$, $HPD_{0.02\text{-}BMLD}$, $HPD_{MLD\text{-}BMLD}$, BMLD and Max N^2) with DCMs and the vertical distribution of Chl-a are described.

3.1 Vertical distribution of DCM and density levels

Deep Chl-a maxima (DCMs) were compared to different structures of the density profile that are summarized in surface mixed layer depth ($MLD_{0.01}$, $MLD_{0.02}$, MLD), bottom mixed layer depth (BMLD), the centre of the pycnocline ($HPD_{0.01\text{-}BMLD}$, $HPD_{0.02\text{-}BMLD}$, $HPD_{MLD\text{-}BMLD}$) and the depth of maximum buoyancy frequency squared (Max N^2) to evaluate i) the vertical distribution of Chl-a above and below each DL, ii) the strength of a positive linear relationship between each DL and DCM, and iii) the prediction of DCM from each DL.

The observations carried out in the FoF and Tay region confirmed the subsurface presence of maxima Chl-a between April and August, with DCMs distributing on average (± standard deviation) at 19.29 ± 6.56 m. All the indicator classifying the surface mixed layer ($MLD_{0.01}$, $MLD_{0.02}$ and MLD) distributed generally shallower than DCMs (Figure 4 a-c, Table 3) with a rare coincidence of their vertical distribution (from 0.39% to 1.73% of the profiles, Table 3). In particular, the thresholds' methods used to identify MLD exhibited the lowest Spearman correlation amongst all DLs, having almost a zero correlation to DCMs (ρ_S = -0.01 and 0.08 for $MLD_{0.01}$ and $MLD_{0.02}$, Table 3) and a limited contribution to define DCM's variability in empirical linear regressions (R^2_{em} = 0.00 and 0.01, Table 3). The major axis regression measured intercepts and slopes in $MLD_{0.01}$ and $MLD_{0.02}$ almost perpendicular to the y-axis due to the strong presence of DCMs in deep waters. Although a clear subsurface aggregation of Chl-a maxima occurs below the surface mixed layer (Figure 4 c), the MLD identified by the algorithm presented in this study correlated better to DCM than $MLD_{0.01}$ and $MLD_{0.02}$, with a positive linear relationship between the two variables and a greater explained variance of DCM by the one-to-one and empirical linear regressions (Table 3). The coefficients of the major axis fitted line for MLD (Table 3) reported a positive correlation of DCMs, representing a gradual deepening of DCM with the top of the pycnocline.

Max N^2 is the density level performing least well after MLDs in predicting DCMs, although it showed the highest percentage of coincidence with DCMs (13.51% of the profiles, Table 3). Similar to MLDs, DCMs have been recorded in 64.96% of the profiles at layers deeper than Max N^2, indicating that Chl-a maxima area located in waters below surface mixing, below stratified layers within the pycnocline.

Overall, the centre of the pycnocline (HPDs) performed better than MLD and Max N^2, distributing closer to DCMs. $HPD_{MLD\text{-}BMLD}$ reported the highest correlation to DCMs (ρ_S = 0.56), and the highest explained DCM's variance from the one-to-one (R^2_0 = 0.90) and empirical (R^2_{em} = 0.31) linear regressions (Table 3). The location of DCMs is highly related to $HPD_{MLD\text{-}BMLD}$, although only 4.63% of the profiles presented DCMs and $HPD_{MLD\text{-}BMLD}$ at the same depth (Table 3). Many profiles exhibited DCM deeper than $HPD_{MLD\text{-}BMLD}$ (78.69%), of which 81.53% distributed DCMs above BMLD (hence, between $HPD_{MLD\text{-}BMLD}$ and BMLD). $HPD_{0.01\text{-}BMLD}$, $HPD_{0.02\text{-}BMLD}$ less related to DCMs in Spearman's correlation, MA, one-to-one and empirical linear regressions than the $HPD_{MLD\text{-}BMLD}$ (Table 3).

The BMLD exhibited a reverse condition compared to the other density levels by encompassing 78.32% of DCMs in waters above it (Table 3). BMLDs is the second variable after $HPD_{MLD\text{-}BMLD}$ with the highest correlation to DCMs (ρ_S = 0.55). It is distributed at the same depth of DCMs in 7.86% of the profiles and linearly predicted the location of maxima Chl-a in both one-to-one and empirical linear regressions (Table 3). BMLD exhibited major axis coefficients (α = 0.60 and β = 0.82) close to the hypothesized one-to-one fitting-line (α = 0 and β = 1), indicating a good approximation of DCMs close to the base of the pycnocline. Moreover, DCMs distributed on average at 2.74 ± 5.21 m above BMLD, with a maximum distance above it equal to 22 m, and 27 m below it.

The overall distribution of DCMs is discernible mainly (> 95.84% of profiles) below the surface mixed layers (MLDs' indicators), within the deepest half of the pycnocline (between $HPD_{MLD\text{-}BMLD}$ and BMLD) and it is bounded for 78.32% of the observations above the BMLD. Although DCMs generally reflect the region with the highest concentration of Chl-a throughout the water column, the vertical distribution of Chl-a can vary in the proximity of DCMs and accumulate mainly above or below it. Hence, the proximity of the density levels (DLs) to DCMs has been investigated along with the vertical distribution of Chl-a (Section 3.2).

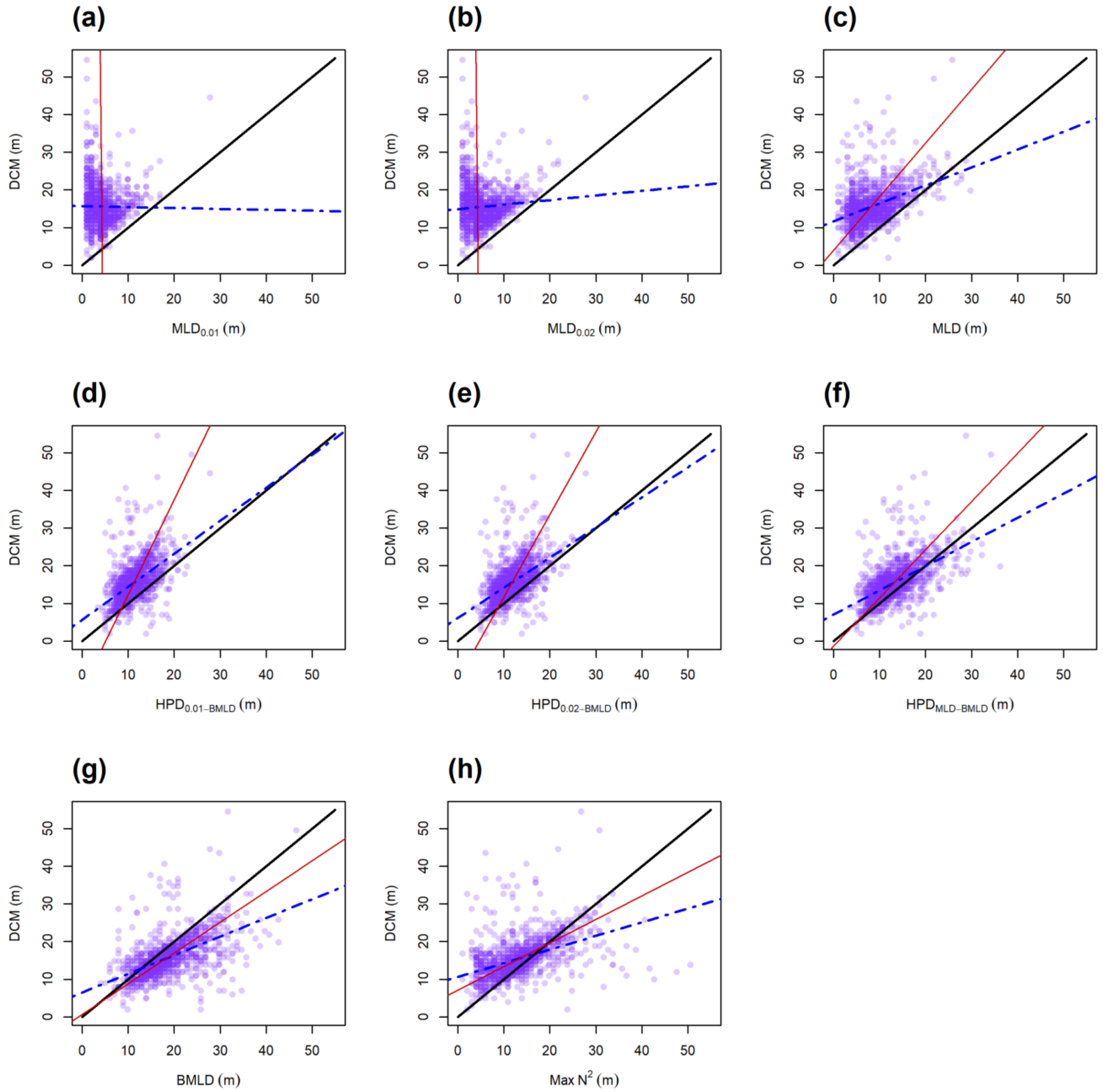

Figure 4: scatterplots on the locations of DCM and the eight density levels (a-h). The lines refer to the one-to-one linear regression (solid black), the major axis regression (solid red), the empirical linear regression measured from the observations (DCM ~ DL) (dot-dashed blue). A good relationship between DL and DCM exhibits similar slope and intercept to the solid black line.

Table 3: statistical parameters and percentage of profiles having DCMs above (>), at the same depth (=), or below (<) each DL. A good relationship is described by an α ~ 0 and β ~ 1, high values of ρ_S, R_0^2, and R_{em}^2. In bold the density levels reporting most coinciding with subsurface Chl-a maxima.

DL	ρ_S	α	β	R_0^2	R_{em}^2	DCM > DL	DCM = DL	DCM < DL
$MLD_{0.01}$	- 0.01	543.35	-124.26	0.40	0.00	99.53	0.39	0.08
$MLD_{0.02}$	0.08	-43.72	11.35	0.47	0.01	99.45	0.31	0.24
MLD	0.41	4.01	1.42	0.69	0.17	95.84	1.73	2.44

$HPD_{0.01\text{-}BMLD}$	0.52	-12.81	2.52	0.86	0.27	90.18	1.81	8.01
$HPD_{0.02\text{-}BMLD}$	0.52	-10.20	2.19	0.87	0.27	86.41	3.77	9.82
$HPD_{MLD\text{-}BMLD}$	**0.56**	**1.31**	**1.28**	**0.90**	**0.31**	**74.86**	**4.63**	**20.50**
BMLD	**0.55**	**0.60**	**0.82**	**0.87**	**0.31**	**13.83**	**7.86**	**78.32**
Max N^2	0.45	7.06	0.63	0.84	0.20	64.96	13.51	21.52

3.2 Chl-a vertical distribution in relation to density levels

Although DCMs generally reflect the region with the highest concentration of Chl-a throughout the water column, large concentration can still accumulate above or below it. Hydrodynamic and biological conditions generating resuspension, passive drift, and mortality (i.e. zooplankton grazing in stratified waters) can shape Chl-a differently throughout the water column. Hence, the relevance of the density levels has been investigated in comparison with the vertical distribution of Chl-a.

The sum of depth-integrated Chl-a (mg m^{-2}) of all profiles was standardized by the number of sampling intervals (m) above and below four DLs (MLD, $HPD_{MLD\text{-}BMLD}$, BMLD and Max N^2). MLD and $HPD_{MLD\text{-}BMLD}$ were selected amongst the density levels to represent the surface mixed layer and the centre of pycnoclines because of their better correlation to DCM (Table 3). The total amount of Chl-a above and below the four density levels is reported as standardized depth-integrated values in Table 4 and shown at each meter depth in Figure 5.

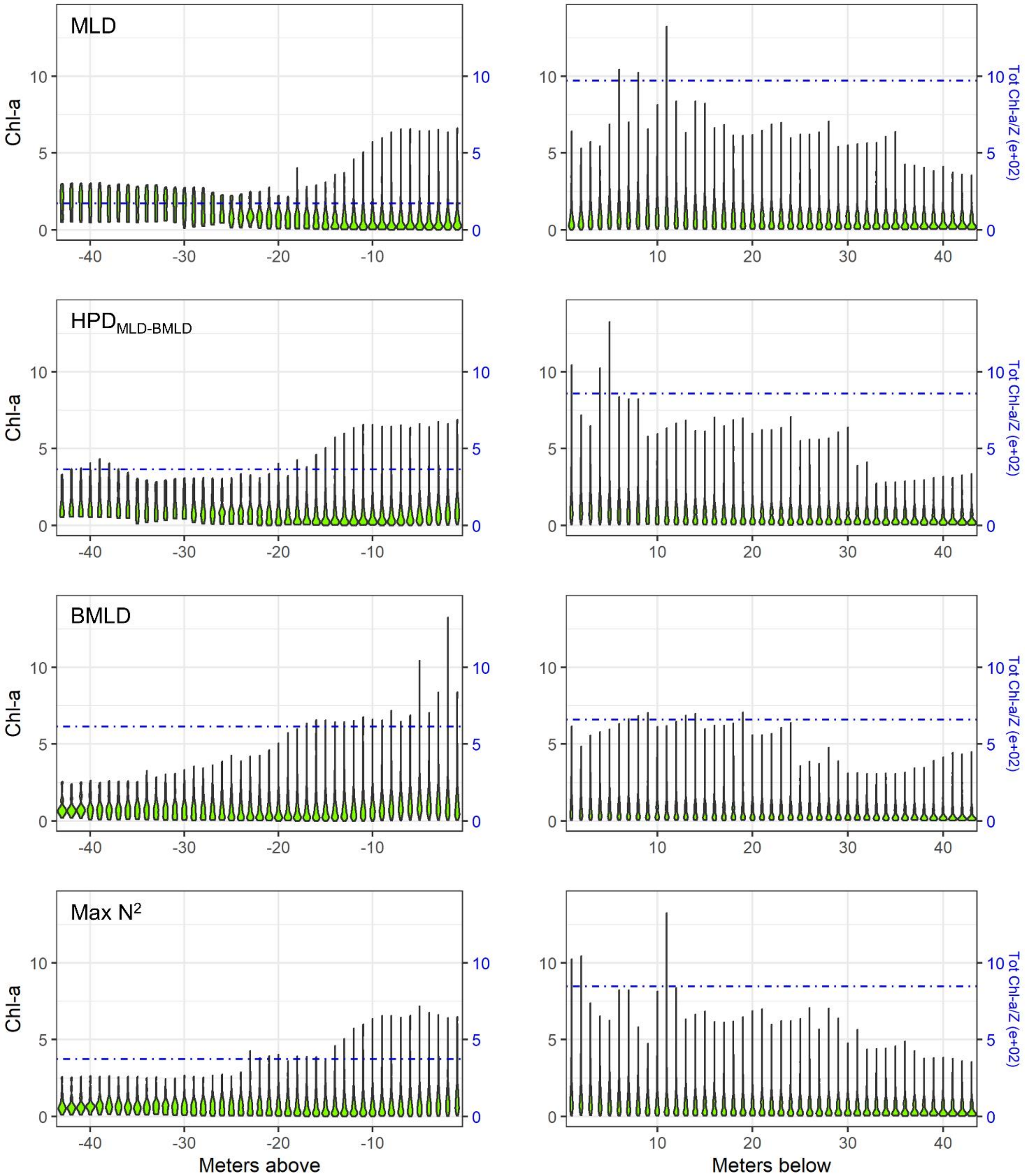

Figure 5: violin plot of Chl-a (mg m^{-3}) at each sampled depth above and below the four density levels (MLD, $HPD_{MLD-BMLD}$, BMLD and Max N^2) for the whole dataset. The dot-dashed blue lines represent the standardized depth-integrated Chl-a measured as the total amount of Chl-a from all profiles (mg m^{-2}) divided by the number of sampling intervals above or below DLs.

Table 4: sum of all depth-integrated Chl-a (mg m^{-2}) standardized by the number of observations above and below the four density layers.

DL	Overall standardized depth-integrated Chl-a above DL (mg m^{-3})	Overall standardized depth-integrated Chl-a below DL (mg m^{-3})
MLD	172.97	971.12
$HPD_{MLD\text{-}BMLD}$	366.07	859.27
BMLD	615.92	658.72
Max N^2	372.90	848.14

Following the results in Section 3.1, a large portion of Chl-a was measured at depths below MLD, $HPD_{MLD\text{-}BMLD}$ and Max N^2 (Table 4), where deep Chl-a maxima also occurred. From the seabed to $HPD_{MLD\text{-}BMLD}$ and Max N^2, the amount of Chl-a was three times than the concentrations within the surface and these DLs. A reverse condition occurred for Chl-a distributing above and below BMLDs: the standardized depth-integrated Chl-a is higher above BMLDs, although the amount of Chl-a in the deepest layers (below the pycnocline) is still comparable (the difference between Chl-a from the surface to BMLD and from BMLD to seabed is 42.80 mg m^{-1}) (Table 4).

It is therefore sensible to infer the distribution of DCMs, and the largest portion of Chl-a, at depths enclosed within the stratified region (MLD-BMLD), especially in the second half of the pycnocline ($HPD_{MLD\text{-}BMLD}$-BMLD). At the same time, a noticeable amount of Chl-a still distributes below the pycnocline (BMLD).

4. Discussion

In stratified waters, the vertical distribution of Chl-a is regulated by the balance of stratification and mixing across different hydrodynamic regimes over time (van Leeuwen et al., 2015). The combination of static, dynamic and biological factors (e.g. grazing, Benoit-Bird et al., 2013) induces phytoplankton communities to adapt their vertical distribution at small scales (< 1 km, Scott et al., 2010; Sharples et al., 2013). Identifying indicators of subsurface Chl-a is essential to investigate the impacts of physical changes due to large-scale factors (e.g. stratification strength, sea level rise, or turbulence increase downstream wind turbine foundations). To date several studies have identified the mixed layer between the sea surface and the pycnocline as a valuable tool to assess changes in phytoplankton abundance and phenology, although MLD lacks the ability to inform the location of subsurface Chl-a in shelf waters. Here we propose a tool to identify the vertical limits of the pycnocline and indicate the bottom mixed layer depth (BMLD) as a key variable influencing the vertical distribution, abundance and phenology of Chl-a in shelf waters.

It is worth noting that the comparison between any DL and DCM was made independent of the time scales at which physical processes and phytoplankton dynamics develop, which differ from each other and do not necessarily overlap. Therefore, the association of any DL with DCM (e.g. BMLD=DCM) was investigated under different physical (e.g. water column stability) and biological conditions (e.g. cell's light history regulating photoacclimation) which are likely to be responsible for the unexplained variance reported for each linear comparison in Figure 4. As an example, the small association of DCMs with all the investigated surface mixed layers' indicators ($MLD_{0.01}$, $MLD_{0.02}$ and MLD, Table 3) can relate to temporal aspects of the phytoplankton dynamic and physical data set (e.g. multiple data collection within oligotrophic surface waters in stably stratified conditions after spring blooms) at the time of sampling. Hence, the association between any DL and DCM would vary depending on the progression of events defining the profiles of Chl-a and density. Here, we discussed the location of DCMs in regard to MLD, HPD, BMLD and Max N^2, considering the potential physical conditions and phytoplankton dynamics at the sampling time (such as water column stability, light history exposure and turbulence) as possible drivers of the resulting associations.

4.1 Association of MLD and Max N^2 with DCMs

Oceanic sites often exhibited phytoplankton blooms within the upper mixed layer (e.g. Behrenfeld, 2010; Costa et al., 2020; Somavilla et al., 2017). Vertical fluctuations of MLD were associated with surface phytoplankton blooms caused by the seasonal stratification of temperate waters (Behrenfeld, 2010) or windstorm events deepening the pycnocline into nutrient-enriched waters (Montes-Hugo et al., 2009; Detoni et al., 2015; Carranza et al., 2018; Höfer et al., 2019). Phytoplankton is known to distribute at the subsurface after blooms, below surface oligotrophic waters (Cullen, 2015), where most of the nutrient input comes from the bottom mixed layer and drives phytoplankton biomass to accumulate at the pycnocline. Since the analysed data in the FoF and Tay region reported DCMs close to the surface (< 14 m) in less than 20% of the profiles, the weak association of DCMs with all the investigated surface mixed layers' indicators ($MLD_{0.01}$, $MLD_{0.02}$ and MLD) can be due to the prevalence of subsurface patches in the dataset, which are likely to be defined by physical dynamics in the bottom rather than the surface mixed layer. In this context, the algorithm returned a measure of the MLD that correlated more with DCMs (ρ_S = 0.41) than $MLD_{0.01}$ and $MLD_{0.02}$ (Table 3), the last distributing above DCMs in > 99% of the profiles. MLD has been considered as a central variable for understanding phytoplankton dynamics in oceanic sites (Sverdrup, 1953), where MLD is mainly informative for surface phytoplankton blooms (Behrenfeld, 2010). This study has shown there is a need for an indicator of the upper limit of the bottom mixed layer, such as BMLD, that would assist further investigation in highly productive but spatially heterogeneous areas such as temperate shelf seas with extensive subsurface aggregations of Chl-a.

In the FoF and Tay region, Max N^2 exhibited higher percentages of coincidence with DCMs (13.51% of 1273 profiles) than other DLs (Table 3). The depth of Max N^2 is a less turbulent region where the energy to exchange parcels in the vertical is maximum (Boehrer and Schultze, 2009). The location of DCMs at Max N^2 might reflect the distribution of phytoplankton within a less turbulent region where resuspended nutrients by upward fluxes from the bottom mixed layer can persist for longer time periods. The Max N^2 would therefore represent a mild turbulent layer where resuspended phytoplankton cells accumulate, while mixing processes above and/or below Max N^2 redistribute phytoplanktonic organisms throughout the water column. However, the amount of standardized depth-integrated Chl-a below Max N^2 is almost three times higher than above it (Table 4 and Figure 5) suggesting that Max N^2 is a small layer of suitable conditions for phytoplankton to grow, but it lacks informing where most of the Chl-a vertically distribute. Although the depth of Max N^2 appeared to better inform the exact location of DCMs, the percentage of its coincidence with DCMs is still low and might relate to specific conditions at the sampling time (physics and phytoplankton dynamics). Overall, the linear correlation (ρ_S), the major axis coefficients and the one-to-one linear regression R_0^2 described a poor association of DCMs with Max N^2 compared to HPD indicators and BMLD, and hence the use of Max N^2 to locate subsurface Chl-a patches in summertime shelf waters may lead to underestimate the amount of Chl-a in the whole water column.

4.2 Vertical distribution of Chl-a and BMLD

The observations carried out in the FoF and Tay region confirmed the subsurface presence of maxima Chl-a between April and August, which typically develop between the spring and autumn blooms in temperate waters. A study in the German Bight described DCMs located mainly at the centre of the pycnocline and the overall amount of Chl-a at depths distinctly lower than the surface mixed layers (Zhao et al., 2019). The location of DCM at the pycnocline typically occurs after blooming events deplete nutrients at the surface (Carranza et al., 2018), and is sustained over time by upward nutrient-enriched fluxes entering the pycnocline from deep waters (Pingree et al., 1982; Rosenberg et al., 1990), which are regulated by tidal currents in shelf seas (Palmer et al., 2008). In the Skagerrak strait between Denmark and Norway, deep SCMs were recorded at a nutricline (rate of change in nitrate and phosphate) located below the base of a shallow pycnocline (< 15 m) (Bjørnsen et al., 1993). In the FoF and Tay region, only 13.83% of the profiles reported DCMs below BMLD (Table 3), suggesting that either grazing (Benoit-Bird et al., 2013) and/or the deep mixing would erode the SCM and redistribute phytoplankton into the bottom mixed layer (Zhao et al., 2019; Sharples et al., 2001).

The erosion and resuspension of phytoplankton in deep turbulent waters occurring in the proximity of BMLD, along with the advection of nutrient-enriched waters sustaining new subsurface production, is likely to play a key role in the carbon fluxes of shelf ecosystems (Sharples et al., 2001). Vertical fluctuations of BMLD within and outside the euphotic zone might define whether resuspended cells in the bottom mixed layer are able to photosynthesize under turbulent and low light conditions, e.g. dinoflagellates with swimming velocity < 0.1 mm s^{-1} are able to compete successfully in slightly turbulent conditions (Ross and Sharples, 2007). However, it is important to note that high concentrations of Chl-a at DCM in dark waters might reflect the photoacclimation of phytoplankton to low light conditions rather than an actual increase in carbon biomass (Marañón et al., 2021). Photoacclimation is a physiological response to light availability and environmental conditions (Masuda et al., 2021), such as variations to vertical mixing (McLaughlin et al., 2020). Hence, the location of DCM close to the base of the pycnocline informs on a large concentration in pigments rather than in carbon production.

4.3 Using BMLD to investigate ecosystem impacts

In this section, the role of BMLD in further studies is introduced. The linkage between the bottom half of the pycnocline (between $HPD_{MLD\text{-}BMLD}$ and BMLD) and subsurface Chl-a advocates BMLD as a key variable to address the physical changes in the bottom mixed layer (below the pycnocline), such as those caused by climate changes (e.g. sediment resuspension, shifts in phytoplankton communities and stratification strengthening) and man-made structures (e.g. increased mixing downstream wind turbine foundations). Identifying BMLD in density profiles would allow measuring the halfway depth of pycnoclines (HPDs), which highly correlated to DCMs (ρ_S = 0.56, Table 3) (Holligan et al., 1984; Sharples et al., 2001), and investigating the effects of physical changes on the abundance, vertical distribution, and species composition of primary producers, grazing and predator species. Further studies would investigate whether pelagic feeders use different structures of the pycnocline (e.g. MLD and BMLD) to detect food patches while diving (e.g. seabirds), and therefore if the variation of these might affect their foraging success.

Climate change

Since deep turbulent processes sustain primary production in shelf waters under prolonged stratified conditions, changes in the vertical distribution of BMLD can be used to inform on the effects of intensified stratification in shelf waters (Capuzzo et al., 2018) such as on the marine food web and physical processes affecting the benthos. The Northeast Atlantic shelves experienced a summertime increase in stratification (increased difference between surface and bottom temperature) with a reduction of nutrient-enriched upward fluxes and a consequential reduction of Chl-a in the last 60 years (Capuzzo et al., 2018; Schmidt et al., 2020). Prolonged stratified conditions are known to promote subsurface patches of Chl-a (Cullen, 2015) due to the depletion of nutrients at the sea surface after blooms. In the Firth of Forth and Tay region, subsurface concentrations (DCMs) distributed in the proximity of the deepest portion of the pycnocline, between $HPD_{MLD\text{-}BMLD}$ and BMLD (78.32% of the profiles), where the weak upward fluxes of nutrients from deep layers are known to sustain the production of Chl-a during summer. The limited nutrients at the surface forces phytoplankton to re-distribute in the water column (e.g. Boyd et al., 2015; Schmidt et al., 2020) and to photosynthesize in deeper nutrient-enriched waters, typically above the bottom mixed layer and within the euphotic zone. Hence, the role of BMLD as a region of the water column with low turbulence and nutrient-enriched upward fluxes (from the bottom mixed layer) is crucial for phytoplankton productivity within the euphotic zone. The combination of a prolonged stratification over time (Capuzzo et al., 2018), a prolonged isolation of surface from deep waters, and an increased sediment load (Capuzzo et al., 2015) associated with climate change might affect the vertical distribution of both the pycnocline and the euphotic zone across time and space, consequentially changing the vertical distribution, abundance and community composition of primary production (Holt et al., 2016, 2018; Capuzzo et al., 2018). The effects of an intensified stratification on primary production suggest an overall reduction of phytoplankton biomass (due to less blooms and mixing events after prolonged stratified conditions) and the settlement of Chl-a at the subsurface, which is likely to delineate a knock-on effect on redistributing most of the higher trophic levels (e.g., zooplankton, fish) and on changing the foraging success of highly adapted species such as surface feeding seabirds (OSPAR, 2017). Identifying the region (such as between $HPD_{MLD\text{-}BMLD}$ and BMLD) at which subsurface DCMs typically distribute is therefore important to investigate the potential effects on the ecosystem. For example, the potential deepening of BMLD below the euphotic zone for extended periods will confine deep nutrients from surface euphotic waters, leading phytoplankton biomass to decrease across shelf seas due to the buoyancy of cells at darker depths or in shallow oligotrophic waters. The persistency of stratified conditions is also likely to change the community composition setting at the subsurface close to BMLD, favouring e.g. species coping with low light availability (in a scenario with increased sediment loads). Hence, the region between $HPD_{MLD\text{-}BMLD}$ and BMLD might represent a key section to sample and investigate potential changes related to the composition of phytoplankton and grazers communities. Moreover, the deepening of productive patches might underestimate the global esteem of primary production since remote sensing methods often lack reliability for subsurface data (Jacox et al., 2015), and global carbon sequestration estimates have often failed to include 10% to 40% of subsurface Chl-a (Sharples et al., 2001). Since the correct measurement of primary production throughout the whole water column is essential, key drivers of subsurface production are demanded to correctly predict, measure, and estimate DCMs from widely used remote sensing data. Although data on the nutricline position were unavailable in this study, the vertical distribution of BMLD informed adequately on the position of productive subsurface patches in stratified waters, making this variable an important indicator of the vertical distribution of phytoplankton in shelf regions.

Offshore renewable infrastructures

It is reasonable to stress that potential effects on primary production involve both surface and deep (below the pycnocline) processes, especially where multiple local changes (i.e. close to wind turbine foundations) repeated over large areas (i.e. the North Sea) can have an effect at different scales (van der Molen et al., 2014; De Dominicis et al., 2018; Carpenter et al., 2016). The upcoming interest of the offshore renewable sector in building offshore wind farms in stratified regions rises the need of drafting reliable environmental impact assessments able to identify key variables for estimating the effects in a holistic way (Dorrell et al., 2022). The consequences of offshore wind farms are likely to be related to bathymetry and mixing budgets, by affecting the stratification rate differently across water depths. In this study area with spring tidal speeds < 1 ms^{-1} , the vertical distribution of DCMs at BMLDs appeared to be correlated to the bathymetry by exhibiting DCMs closer to BMLDs at water depths comprised from, approximately, 40 to 70 m, DCMs deeper than BMLD mainly in shallow waters < 60 m, and DCMs above BMLD towards deeper waters up to 100 m (Figure A3 in Appendix A). Previous studies identified a similar pattern in shallow waters (25-85 m) where DCMs were mainly recorded at or below the base of the pycnocline (Barth et al., 1998; Durán-Campos et al., 2019; Holligan et al., 1984; Zhao et al., 2019). Although stratification is reported to intensify in shelf waters with climate change (Capuzzo et al., 2018), the increase in turbulence downstream of wind turbine foundations may counteract the local stratification (Carpenter et al., 2016; Schulien et al., 2017; Schultze et al., 2020) and affect the vertical distribution and thickness of the pycnocline across time and space. Moreover, the bouncy of floating wind turbines within the upper water layer (≈ 25 m) will impact the mixing across density interfaces (Dorrell et al., 2022), and BMLD might represent a useful indicator to vertically locate, on a large-scale, small-scales processes such as scouring and overturning (see Caulfield, 2021). Since the variation in stratification is a useful tool to address possible impacts on primary production, understanding the potential impacts on the vertical distribution of BMLD due to wind turbine foundations, and of MLD due to wind extraction (Daewel et al., 2022), is likely to efficiently predict changes in the vertical distribution of Chl-a and its possible predators.

5. Conclusion

The mixing processes above and below the pycnocline can have very different influences on Chl-a vertical distribution, dictating the distribution of subsurface concentrations close to, above, or below the pycnocline. The extent to which subsurface Chl-a maxima distribute in the proximity of any density level was investigated aside from any variable controlling for the progression of events affecting the physics and biological dynamics of the water column (e.g. vertical Chl-a shape or water column stability) at the sampling time. Hence, the extent of variability retrieved from each comparison (e.g. DCM close to BMLD) is most likely related to the different conditions under which the water columns were investigated, such as the vertical distribution of Chl-a (shapes), nutrients availability, stability of the water column (transition from either stratified to mixed condition or *vice versa*), tidal phase, grazing factors, phytoplankton dynamics (e.g. cell's light history, species composition and competition).

MLD would distribute close to DCMs during surface blooms, explaining the small correlation between MLD and subsurface Chl-a in the FoF and Tay region, where a small portion of surface Chl-a (< 15 m) was collected between 2000 and 2014 (less than 20% of the profiles). The results indicate that summertime subsurface Chl-a maxima distribute close to HPD and BMLD, indicating that deep processes boosting mixing (such as tidal currents in the North Sea) regulate summer primary production and most of the production above and below BMLDs in, respectively, deep and shallow waters. Further studies reported the key role of the bottom mixed layer in regulating subsurface production and carbon fluxes (Sharples et al., 2001; Palmer et al., 2008), advocating BMLD as vertical depth where the effects of anomaly-inducing processes (e.g. reduced oxygen concentrations below the pycnocline) need to be further investigated. The designed approach is being developed in order to help the identification of broad linkages between the physical environment and primary production at finer spatial scales (≤ 1 km), and a tool to extrapolate this variable from high-resolution vertical profiles in stratified waters is proposed.

Appendix A

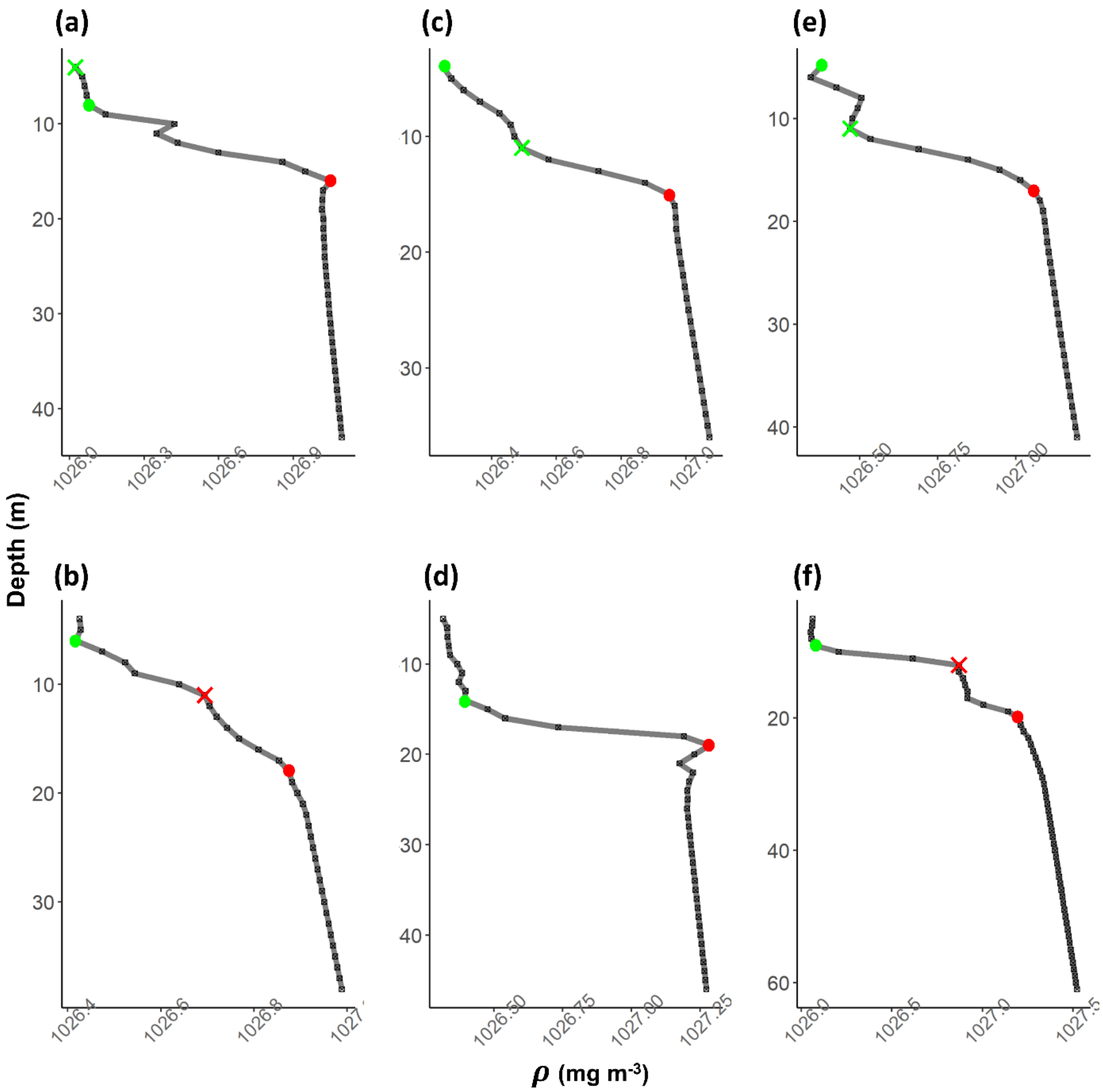

670 *Figure A1: examples of density profiles (grey line) (a-f). The black squares are observations at 1 m resolution. Red dots refer to BMLD, green dots to MLD. Crosses refer to misidentified MLD (in green) and BMLD (in red) that were manually corrected.*

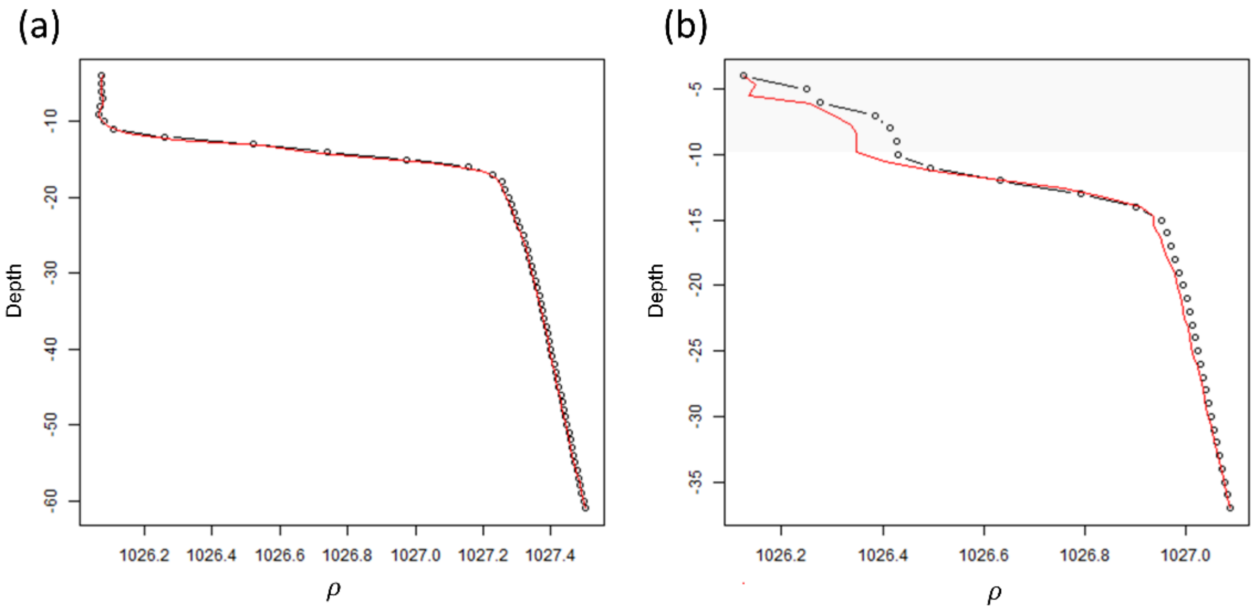

Figure A2: two density profiles whose observations were standardized at equals 1 m intervals using generalized additive model (GAM). (a) density profile (black dotted line) where the GAM correctly fitted (red solid line) the vertical distribution. (b) density profile where the GAM wrongly fitted the upper portion of the profile (grey polygon area) and, hence, required a manual correction of the values.

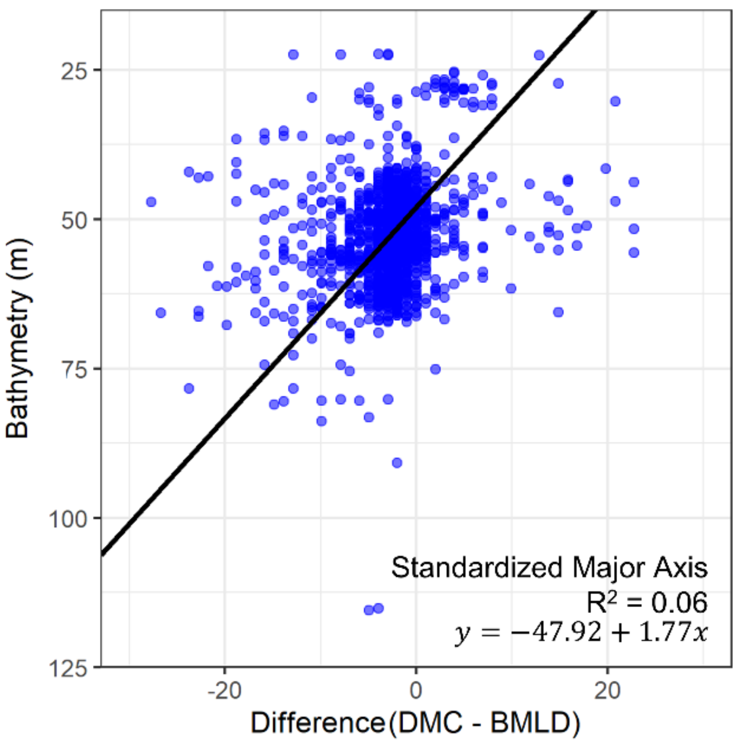

Figure A3: scatterplot of the difference between DCM and BMLD against the bathymetry at which each profile was sampled. The solid black line reports a standardized major axis regression, whose equation and R squared values are reported.

Author contribution

Arianna Zampollo contributed to the conceptualization of the study, formal analyses, methodology on MLD and BMLD, writing and reviewing the paper, and software use; Thomas Cornulier contributed to the conceptualization and supervision of the statistical method, writing of the original draft, methodology and visualization of the results; Rory O'Hara Murray contributed on the data curation, writing of the original draft, supervision, visualization and validation; Jacqueline F. Tweddle contributed to the conceptualization and the supervision of the study; James Dunning contributed to the methodology of the MLD and BMLD algorithm; Beth Scott contributed to the conceptualization of the analyses, writing of the original draft, revisions, contextualization and discussion of the results, supervision, funding acquisition, resources and data curation.

Code availability

The codes for the identification of DCM, MLD and BMLD are available at https://github.com/azampollo/BMLD

Data availability

Data are available upon request and agreement with the co-authors.

Competing interests

The authors declare that they have no conflict of interest.

Acknowledgment

The authors thank the founding MarCRF, the Marine Collaboration Research Forum jointly sponsored by the University of Aberdeen and Marine Scotland Science, and Marine Scotland Science to provide the CTD data.

References

Baetge, N., Graff, J. R., Behrenfeld, M. J., and Carlson, C. A.: Net Community Production, Dissolved Organic Carbon Accumulation, and Vertical Export in the Western North Atlantic, Front. Mar. Sci., 7, 227, https://doi.org/10.3389/fmars.2020.00227, 2020.

Barth, J. A., Bogucki, D., Pierce, S. D., and Kosro, P. M.: Secondary circulation associated with a shelfbreak front, Geophys. Res. Lett., 25, 2761–2764, https://doi.org/10.1029/98GL02104, 1998.

Behrenfeld, M. J.: Abandoning Sverdrup's Critical Depth Hypothesis on phytoplankton blooms, Ecology, 91, 977–989, https://doi.org/10.1890/09-1207.1, 2010.

Benoit-Bird, K. J., Shroyer, E. L., and McManus, M. A.: A critical scale in plankton aggregations across coastal ecosystems: CRITICAL SCALE IN PLANKTON AGGREGATIONS, Geophys. Res. Lett., 40, 3968–3974, https://doi.org/10.1002/grl.50747, 2013.

Bjørnsen, P., Kaas, H., Kaas, H., Nielsen, T., Olesen, M., and Richardson, K.: Dynamics of a subsurface phytoplankton maximum in the Skagerrak, Mar. Ecol. Prog. Ser., 95, 279–294, https://doi.org/10.3354/meps095279, 1993.

Boehrer, B. and Schultze, M.: Density Stratification and Stability, in: Encyclopedia of Inland Waters, edited by: Likens, G. E., Academic Press, Oxford, 583–593, https://doi.org/10.1016/B978-012370626-3.00077-6, 2009.

Bonaduce, A., Staneva, J., Behrens, A., Bidlot, J.-R., and Wilcke, R. A. I.: Wave Climate Change in the North Sea and Baltic Sea, J. Mar. Sci. Eng., 7, 166, https://doi.org/10.3390/jmse7060166, 2019.

Boyd, P. W., Lennartz, S. T., Glover, D. M., and Doney, S. C.: Biological ramifications of climate-change-mediated oceanic multi-stressors, Nat. Clim. Change, 5, 71–79, https://doi.org/10.1038/nclimate2441, 2015.

Brown, Z. W., Lowry, K. E., Palmer, M. A., van Dijken, G. L., Mills, M. M., Pickart, R. S., and Arrigo, K. R.: Characterizing the subsurface chlorophyll a maximum in the Chukchi Sea and Canada Basin, Deep Sea Res. Part II Top. Stud. Oceanogr., 118, 88–104, https://doi.org/10.1016/j.dsr2.2015.02.010, 2015.

Capuzzo, E., Stephens, D., Silva, T., Barry, J., and Forster, R. M.: Decrease in water clarity of the southern and central North Sea during the 20th century, Glob. Change Biol., 21, 2206–2214, https://doi.org/10.1111/gcb.12854, 2015.

Capuzzo, E., Lynam, C. P., Barry, J., Stephens, D., Forster, R. M., Greenwood, N., McQuatters-Gollop, A., Silva, T., Leeuwen, S. M. van, and Engelhard, G. H.: A decline in primary production in the North Sea over 25 years, associated with reductions in zooplankton abundance and fish stock recruitment, Glob. Change Biol., 24, e352–e364, https://doi.org/10.1111/gcb.13916, 2018.

Carpenter, J. R., Merckelbach, L., Callies, U., Clark, S., Gaslikova, L., and Baschek, B.: Potential Impacts of Offshore Wind Farms on North Sea Stratification, PLOS ONE, 11, e0160830, https://doi.org/10.1371/journal.pone.0160830, 2016.

Carranza, M. M., Gille, S. T., Franks, P. J. S., Johnson, K. S., Pinkel, R., and Girton, J. B.: When Mixed Layers Are Not Mixed. Storm-Driven Mixing and Bio-optical Vertical Gradients in Mixed Layers of the Southern Ocean, J. Geophys. Res. Oceans, 123, 7264–7289, https://doi.org/10.1029/2018JC014416, 2018.

Carvalho, F., Kohut, J., Oliver, M. J., and Schofield, O.: Defining the ecologically relevant mixed-layer depth for Antarctica's coastal seas, Geophys. Res. Lett., 44, 338–345, https://doi.org/10.1002/2016GL071205, 2017.

Caulfield, C. P.: Layering, Instabilities, and Mixing in Turbulent Stratified Flows, Annu. Rev. Fluid Mech., 53, 113–145, https://doi.org/10.1146/annurev-fluid-042320-100458, 2021.

Chiswell, S. M.: Annual cycles and spring blooms in phytoplankton: don't abandon Sverdrup completely, Mar. Ecol. Prog. Ser., 443, 39–50, https://doi.org/10.3354/meps09453, 2011.

Chu, P. C. and Fan, C.: Maximum angle method for determining mixed layer depth from seaglider data, J. Oceanogr., 67, 219–230, https://doi.org/10.1007/s10872-011-0019-2, 2011.

Chu, P. C. and Fan, C.: Global ocean synoptic thermocline gradient, isothermal-layer depth, and other upper ocean parameters, Sci. Data, 6, 119, https://doi.org/10.1038/s41597-019-0125-3, 2019.

Costa, R. R., Mendes, C. R. B., Tavano, V. M., Dotto, T. S., Kerr, R., Monteiro, T., Odebrecht, C., and Secchi, E. R.: Dynamics of an intense diatom bloom in the Northern Antarctic Peninsula, February 2016, Limnol. Oceanogr., 65, 2056–2075, https://doi.org/10.1002/lno.11437, 2020.

Courtois, P., Hu, X., Pennelly, C., Spence, P., and Myers, P. G.: Mixed layer depth calculation in deep convection regions in ocean numerical models, Ocean Model., 120, 60–78, https://doi.org/10.1016/j.ocemod.2017.10.007, 2017.

Cullen, J. J.: Subsurface Chlorophyll Maximum Layers: Enduring Enigma or Mystery Solved?, Annu. Rev. Mar. Sci., 7, 207–239, https://doi.org/10.1146/annurev-marine-010213-135111, 2015.

Daewel, U., Akhtar, N., Christiansen, N., and Schrum, C.: Offshore wind farms are projected to impact primary production and bottom water deoxygenation in the North Sea, Commun. Earth Environ., 3, 1–8, https://doi.org/10.1038/s43247-022-00625-0, 2022.

De Dominicis, M., Wolf, J., and O'Hara Murray, R.: Comparative Effects of Climate Change and Tidal Stream Energy Extraction in a Shelf Sea, J. Geophys. Res. Oceans, 123, 5041–5067, https://doi.org/10.1029/2018JC013832, 2018.

Detoni, A. M. S., de Souza, M. S., Garcia, C. A. E., Tavano, V. M., and Mata, M. M.: Environmental conditions during phytoplankton blooms in the vicinity of James Ross Island, east of the Antarctic Peninsula, Polar Biol., 38, 1111–1127, https://doi.org/10.1007/s00300-015-1670-7, 2015.

Diehl, S.: Phytoplankton, Light, and Nutrients in a Gradient of Mixing Depths: Theory, Ecology, 83, 386–398, https://doi.org/10.1890/0012-9658(2002)083[0386:PLANIA]2.0.CO;2, 2002.

Diehl, S., Berger, S., Ptacnik, R., and Wild, A.: Phytoplankton, Light, and Nutrients in a Gradient of Mixing Depths: Field Experiments, Ecology, 83, 399–411, https://doi.org/10.1890/0012-9658(2002)083[0399:PLANIA]2.0.CO;2, 2002.

Dorrell, R. M., Lloyd, C. J., Lincoln, B. J., Rippeth, T. P., Taylor, J. R., Caulfield, C. P., Sharples, J., Polton, J. A., Scannell, B. D., Greaves, D. M., Hall, R. A., and Simpson, J. H.: Anthropogenic Mixing in Seasonally Stratified Shelf Seas by Offshore Wind Farm Infrastructure, Front. Mar. Sci., 9, 2022.

D'Ortenzio, F., Lavigne, H., Besson, F., Claustre, H., Coppola, L., Garcia, N., Laës-Huon, A., Le Reste, S., Malardé, D., Migon, C., Morin, P., Mortier, L., Poteau, A., Prieur, L., Raimbault, P., and Testor, P.: Observing mixed layer depth, nitrate and chlorophyll concentrations in the northwestern Mediterranean: A combined satellite and NO_3 profiling floats experiment, Geophys. Res. Lett., 41, 6443–6451, https://doi.org/10.1002/2014GL061020, 2014.

Ducklow, H. W., Baker, K., Martinson, D. G., Quetin, L. B., Ross, R. M., Smith, R. C., Stammerjohn, S. E., Vernet, M., and Fraser, W.: Marine pelagic ecosystems: the West Antarctic Peninsula, Philos. Trans. R. Soc. B Biol. Sci., 362, 67–94, https://doi.org/10.1098/rstb.2006.1955, 2007.

Durán-Campos, E., Monreal-Gómez, M. A., Salas de León, D. A., and Coria-Monter, E.: Chlorophyll-a vertical distribution patterns during summer in the Bay of La Paz, Gulf of California, Mexico, Egypt. J. Aquat. Res., 45, 109–115, https://doi.org/10.1016/j.ejar.2019.04.003, 2019.

González-Pola, C., Fernández-Díaz, J. M., and Lavín, A.: Vertical structure of the upper ocean from profiles fitted to physically consistent functional forms, Deep Sea Res. Part Oceanogr. Res. Pap., 54, 1985–2004, https://doi.org/10.1016/j.dsr.2007.08.007, 2007.

Gradone, J. C., Oliver, M. J., Davies, A. R., Moffat, C., and Irwin, A.: Sea Surface Kinetic Energy as a Proxy for Phytoplankton Light Limitation in the Summer Pelagic Southern Ocean, J. Geophys. Res. Oceans, 125, e2019JC015646, https://doi.org/10.1029/2019JC015646, 2020.

Hastie, T. J., and Tibshirani, R. J.: *Generalized additive models*. 1st edition, Routledge, https://doi.org/10.1201/9780203753781, 1990.

Hickman, A., Moore, C., Sharples, J., Lucas, M., Tilstone, G., Krivtsov, V., and Holligan, P.: Primary production and nitrate uptake within the seasonal thermocline of a stratified shelf sea, Mar. Ecol. Prog. Ser., 463, 39–57, https://doi.org/10.3354/meps09836, 2012.

Höfer, J., Giesecke, R., Hopwood, M. J., Carrera, V., Alarcón, E., and González, H. E.: The role of water column stability and wind mixing in the production/export dynamics of two bays in the Western Antarctic Peninsula, Prog. Oceanogr., 174, 105–116, https://doi.org/10.1016/j.pocean.2019.01.005, 2019.

Holligan, P. M., Balch, W. M., and Yentsch, C. M.: The significance of subsurface chlorophyll, nitrite and ammonium maxima in relation to nitrogen for phytoplankton growth in stratified waters of the Gulf of Maine, J. Mar. Res., 42, 1051–1073, https://doi.org/10.1357/002224084788520747, 1984.

Holt, J., Schrum, C., Cannaby, H., Daewel, U., Allen, I., Artioli, Y., Bopp, L., Butenschon, M., Fach, B. A., Harle, J., Pushpadas, D., Salihoglu, B., and Wakelin, S.: Potential impacts of climate change on the primary production of regional seas: A comparative analysis of five European seas, Prog. Oceanogr., 140, 91–115, https://doi.org/10.1016/j.pocean.2015.11.004, 2016.

Holt, J., Polton, J., Huthnance, J., Wakelin, S., O'Dea, E., Harle, J., Yool, A., Artioli, Y., Blackford, J., Siddorn, J., and Inall, M.: Climate-Driven Change in the North Atlantic and Arctic Oceans Can Greatly Reduce the Circulation of the North Sea, Geophys. Res. Lett., 45, 11,827-11,836, https://doi.org/10.1029/2018GL078878, 2018.

Holte, J. and Talley, L.: A New Algorithm for Finding Mixed Layer Depths with Applications to Argo Data and Subantarctic Mode Water Formation, J. Atmospheric Ocean. Technol., 26, 1920–1939, https://doi.org/10.1175/2009JTECHO543.1, 2009.

Hopkins, J. E., Palmer, M. R., Poulton, A. J., Hickman, A. E., and Sharples, J.: Control of a phytoplankton bloom by wind-driven vertical mixing and light availability, Limnol. Oceanogr., 66, 1926–1949, https://doi.org/10.1002/lno.11734, 2021.

Jacox, M. G., Edwards, C. A., Kahru, M., Rudnick, D. L., and Kudela, R. M.: The potential for improving remote primary productivity estimates through subsurface chlorophyll and irradiance measurement, Deep Sea Res. Part II Top. Stud. Oceanogr., 112, 107–116, https://doi.org/10.1016/j.dsr2.2013.12.008, 2015.

Klymak, J. M., Pinkel, R., and Rainville, L.: Direct Breaking of the Internal Tide near Topography: Kaena Ridge, Hawaii, J. Phys. Oceanogr., 38, 380–399, https://doi.org/10.1175/2007JPO3728.1, 2008.

van Leeuwen, S. van, Tett, P., Mills, D., and Molen, J. van der: Stratified and nonstratified areas in the North Sea: Long-term variability and biological and policy implications, J. Geophys. Res. Oceans, 120, 4670–4686, https://doi.org/10.1002/2014JC010485, 2015.

Lips, U., Lips, I., Liblik, T., and Kuvaldina, N.: Processes responsible for the formation and maintenance of sub-surface chlorophyll maxima in the Gulf of Finland, Estuar. Coast. Shelf Sci., 88, 339–349, https://doi.org/10.1016/j.ecss.2010.04.015, 2010.

Lloyd, S.: Least squares quantization in PCM, in: *IEEE Transactions on Information Theory*, 28 (2), 129-137, https://ieeexplore.ieee.org/document/1056489, 1982.

Lorbacher, K., Dommenget, D., Niiler, P. P., and Köhl, A.: Ocean mixed layer depth: A subsurface proxy of ocean-atmosphere variability, J. Geophys. Res. Oceans, 111, https://doi.org/10.1029/2003JC002157, 2006.

Lozier, M. S., Dave, A. C., Palter, J. B., Gerber, L. M., and Barber, R. T.: On the relationship between stratification and primary productivity in the North Atlantic, Geophys. Res. Lett., 38, https://doi.org/10.1029/2011GL049414, 2011.

Marañón, E., Van Wambeke, F., Uitz, J., Boss, E. S., Dimier, C., Dinasquet, J., Engel, A., Haëntjens, N., Pérez-Lorenzo, M., Taillandier, V., and Zäncker, B.: Deep maxima of phytoplankton biomass, primary production and bacterial production in the Mediterranean Sea, Biogeosciences, 18, 1749–1767, https://doi.org/10.5194/bg-18-1749-2021, 2021.

Martin, J., Tremblay, J.-É., Gagnon, J., Tremblay, G., Lapoussière, A., Jose, C., Poulin, M., Gosselin, M., Gratton, Y., and Michel, C.: Prevalence, structure and properties of subsurface chlorophyll maxima in Canadian Arctic waters, Mar. Ecol. Prog. Ser., 412, 69–84, https://doi.org/10.3354/meps08666, 2010.

Masuda, Y., Yamanaka, Y., Smith, S. L., Hirata, T., Nakano, H., Oka, A., and Sumata, H.: Photoacclimation by phytoplankton determines the distribution of global subsurface chlorophyll maxima in the ocean, Commun. Earth Environ., 2, 1–8, https://doi.org/10.1038/s43247-021-00201-y, 2021.

McLaughlin, M. J., Greenwood, J., Branson, P., Lourey, M. J., and Hanson, C. E.: Evidence of Phytoplankton Light Acclimation to Periodic Turbulent Mixing Along a Tidally Dominated Tropical Coastline, J. Geophys. Res. Oceans, 125, e2020JC016615, https://doi.org/10.1029/2020JC016615, 2020.

van der Molen, J., Smith, H. C. M., Lepper, P., Limpenny, S., and Rees, J.: Predicting the large-scale consequences of offshore wind turbine array development on a North Sea ecosystem, Cont. Shelf Res., 85, 60–72, https://doi.org/10.1016/j.csr.2014.05.018, 2014.

Montégut, C. de B., Madec, G., Fischer, A. S., Lazar, A., and Iudicone, D.: Mixed layer depth over the global ocean: An examination of profile data and a profile-based climatology, J. Geophys. Res. Oceans, 109, https://doi.org/10.1029/2004JC002378, 2004.

Montes-Hugo, M., Doney, S. C., Ducklow, H. W., Fraser, W., Martinson, D., Stammerjohn, S. E., and Schofield, O.: Recent Changes in Phytoplankton Communities Associated with Rapid Regional Climate Change Along the Western Antarctic Peninsula, Science, 323, 1470–1473, https://doi.org/10.1126/science.1164533, 2009.

Orihuela-Pinto, B., England, M. H., and Taschetto, A. S.: Interbasin and interhemispheric impacts of a collapsed Atlantic Overturning Circulation, Nat. Clim. Change, 12, 558–565, https://doi.org/10.1038/s41558-022-01380-y, 2022.

Palmer, M. R., Rippeth, T. P., and Simpson, J. H.: An investigation of internal mixing in a seasonally stratified shelf sea, J. Geophys. Res. Oceans, 113, https://doi.org/10.1029/2007JC004531, 2008.

Palmer, M. R., Inall, M. E., and Sharples, J.: The physical oceanography of Jones Bank: A mixing hotspot in the Celtic Sea, Prog. Oceanogr., 117, 9–24, https://doi.org/10.1016/j.pocean.2013.06.009, 2013.

Pingree, R. D. and Griffiths, D. K.: The bottom mixed layer on the continental shelf, Estuar. Coast. Mar. Sci., 5, 399–413, https://doi.org/10.1016/0302-3524(77)90064-0, 1977.

Pingree, R. D., Holligan, P. M., Mardell, G. T., and Harris, R. P.: Vertical distribution of plankton in the skagerrak in relation to doming of the seasonal thermocline, Cont. Shelf Res., 1, 209–219, https://doi.org/10.1016/0278-4343(82)90005-X, 1982.

Poulton, A. J., Mazwane, S. L., Godfrey, B., Carvalho, F., Mawji, E., Wihsgott, J. U., and Noyon, M.: Primary production dynamics on the Agulhas Bank in autumn, Deep Sea Res. Part II Top. Stud. Oceanogr., 203, 105153, https://doi.org/10.1016/j.dsr2.2022.105153, 2022.

Prend, C. J., Gille, S. T., Talley, L. D., Mitchell, B. G., Rosso, I., and Mazloff, M. R.: Physical Drivers of Phytoplankton Bloom Initiation in the Southern Ocean's Scotia Sea, J. Geophys. Res. Oceans, 124, 5811–5826, https://doi.org/10.1029/2019JC015162, 2019.

Prézelin, B. B., Hofmann, E. E., Mengelt, C., and Klinck, J. M.: The linkage between Upper Circumpolar Deep Water (UCDW) and phytoplankton assemblages on the west Antarctic Peninsula continental shelf, J. Mar. Res., 58, 165–202, https://doi.org/10.1357/002224000321511133, 2000.

Prézelin, B. B., Hofmann, E. E., Moline, M., and Klinck, J. M.: Physical forcing of phytoplankton community structure and primary production in continental shelf waters of the Western Antarctic Peninsula, J. Mar. Res., 62, 419–460, https://doi.org/10.1357/0022240041446173, 2004.

R Core Team: R Foundation for Statistical Computing. Vienna, Austria, 2018.

Richardson, K. and Pedersen, F. B.: Estimation of new production in the North Sea: consequences for temporal and spatial variability of phytoplankton, ICES J. Mar. Sci., 55, 574–580, https://doi.org/10.1006/jmsc.1998.0402, 1998.

Rosenberg, R., Dahl, E., Edler, L., Fyrberg, L., Granéli, E., Granéli, W., Hagström, Å., Lindahl, O., Matos, M. O., Pettersson, K., Sahlsten, E., Tiselius, P., Turk, V., and Wikner, J.: Pelagic nutrient and energy transfer during spring in the open and coastal Skagerrak, Mar. Ecol. Prog. Ser., 61, 215–231, 1990.

Ross, O. N. and Sharples, J.: Phytoplankton motility and the competition for nutrients in the thermocline, Mar. Ecol. Prog. Ser., 347, 21–38, https://doi.org/10.3354/meps06999, 2007.

Ryan-Keogh, T. J. and Thomalla, S. J.: Deriving a Proxy for Iron Limitation From Chlorophyll Fluorescence on Buoyancy Gliders, Front. Mar. Sci., 7, 275, https://doi.org/10.3389/fmars.2020.00275, 2020.

Schmidt, K., Birchill, A. J., Atkinson, A., Brewin, R. J. W., Clark, J. R., Hickman, A. E., Johns, D. G., Lohan, M. C., Milne, A., Pardo, S., Polimene, L., Smyth, T. J., Tarran, G. A., Widdicombe, C. E., Woodward, E. M. S., and Ussher, S. J.: Increasing picocyanobacteria success in shelf waters contributes to long-term food web degradation, Glob. Change Biol., https://doi.org/10.1111/gcb.15161, 2020.

Schofield, O., Miles, T., Alderkamp, A.-C., Lee, S., Haskins, C., Rogalsky, E., Sipler, R., Sherrell, R. M., and Yager, P. L.: *In situ* phytoplankton distributions in the Amundsen Sea Polynya measured by autonomous gliders, Elem. Sci. Anthr., 3, 000073, https://doi.org/10.12952/journal.elementa.000073, 2015.

Schulien, J. A., Behrenfeld, M. J., Hair, J. W., Hostetler, C. A., and Twardowski, M. S.: Vertically- resolved phytoplankton carbon and net primary production from a high spectral resolution lidar, Opt. Express, 25, 13577, https://doi.org/10.1364/OE.25.013577, 2017.

Schultze, L. K. P., Merckelbach, L. M., Horstmann, J., Raasch, S., and Carpenter, J. R.: Increased Mixing and Turbulence in the Wake of Offshore Wind Farm Foundations, J. Geophys. Res. Oceans, 125, e2019JC015858, https://doi.org/10.1029/2019JC015858, 2020.

Scott, B. E., Sharples, J., Ross, O. N., Wang, J., Pierce, G. J., and Camphuysen, C. J.: Sub-surface hotspots in shallow seas: fine-scale limited locations of top predator foraging habitat indicated by tidal mixing and sub-surface chlorophyll, Mar. Ecol. Prog. Ser., 408, 207–226, https://doi.org/10.3354/meps08552, 2010.

Sharples, J., Moore, M. C., Rippeth, T. P., Holligan, P. M., Hydes, D. J., Fisher, N. R., and Simpson, J. H.: Phytoplankton distribution and survival in the thermocline, Limnol. Oceanogr., 46, 486–496, https://doi.org/10.4319/lo.2001.46.3.0486, 2001.

Sharples, J., Ross, O. N., Scott, B. E., Greenstreet, S. P. R., and Fraser, H.: Inter-annual variability in the timing of stratification and the spring bloom in the North-western North Sea, Cont. Shelf Res., 26, 733–751, https://doi.org/10.1016/j.csr.2006.01.011, 2006.

Sharples, J., Scott, B. E., and Inall, M. E.: From physics to fishing over a shelf sea bank, Prog. Oceanogr., 117, 1–8, https://doi.org/10.1016/j.pocean.2013.06.015, 2013.

Somavilla, R., González-Pola, C., and Fernández-Diaz, J.: The warmer the ocean surface, the shallower the mixed layer. How much of this is true?, J. Geophys. Res. Oceans, 122, 7698–7716, https://doi.org/10.1002/2017JC013125, 2017.

Steinacher, M., Joos, F., Frölicher, T. L., Bopp, L., Cadule, P., Cocco, V., Doney, S. C., Gehlen, M., Lindsay, K., Moore, J. K., Schneider, B., and Segschneider, J.: Projected 21st century decrease in marine productivity: a multi-model analysis, Biogeosciences, 7, 979–1005, https://doi.org/10.5194/bg-7-979-2010, 2010.

Sverdrup, H. U.,: On conditions for the vernal blooming of phytoplankton. J. Cons. Int. Explor. Mer, 18, 287–295, 1953.

Taboada, F. G. and Anadón, R.: Patterns of change in sea surface temperature in the North Atlantic during the last three decades: beyond mean trends, Clim. Change, 115, 419–431, https://doi.org/10.1007/s10584-012-0485-6, 2012.

Takahashi, M. and Hori, T.: Abundance of picophytoplankton in the subsurface chlorophyll maximum layer in subtropical and tropical waters, Mar. Biol., 79, 177–186, https://doi.org/10.1007/BF00951826, 1984.

Thomson, R. E. and Fine, I. V.: Estimating Mixed Layer Depth from Oceanic Profile Data, J. Atmospheric Ocean. Technol., 20, 319–329, https://doi.org/10.1175/1520-0426(2003)020<0319:EMLDFO>2.0.CO;2, 2003.

Walsby, A. E.: Numerical integration of phytoplankton photosynthesis through time and depth in a water column, New Phytol., 136, 189–209, https://doi.org/10.1046/j.1469-8137.1997.00736.x, 1997.

Warton, D. I., Wright, I. J., Falster, D. S., and Westoby, M.: Bivariate line-fitting methods for allometry, Biol. Rev., 81, 259–291, https://doi.org/10.1017/S1464793106007007, 2006.

Weston, K., Fernand, L., Mills, D. K., Delahunty, R., and Brown, J.: Primary production in the deep chlorophyll maximum of the central North Sea, J. Plankton Res., 27, 909–922, https://doi.org/10.1093/plankt/fbi064, 2005.

Wihsgott, J. U., Sharples, J., Hopkins, J. E., Woodward, E. M. S., Hull, T., Greenwood, N., and Sivyer, D. B.: Observations of vertical mixing in autumn and its effect on the autumn phytoplankton bloom, Prog. Oceanogr., 177, 102059, https://doi.org/10.1016/j.pocean.2019.01.001, 2019.

Yentsch, C. S.: Influence of geostrophy on primary production. [Effect of ocean currents on nutrients of ocean water], Tethys Fr., 6:1–2, 1974.

Yentsch, C. S.: Phytoplankton Growth in the Sea, in: Primary Productivity in the Sea, edited by: Falkowski, P. G., Springer US, Boston, MA, 17–32, https://doi.org/10.1007/978-1-4684-3890-1_2, 1980.

Zhang, W.-Z., Wang, H., Chai, F., and Qiu, G.: Physical drivers of chlorophyll variability in the open South China Sea, J. Geophys. Res. Oceans, 121, 7123–7140, https://doi.org/10.1002/2016JC011983, 2016.

Zhao, C., Maerz, J., Hofmeister, R., Röttgers, R., Wirtz, K., Riethmüller, R., and Schrum, C.: Characterizing the vertical distribution of chlorophyll a in the German Bight, Cont. Shelf Res., 175, 127–146, https://doi.org/10.1016/j.csr.2019.01.012, 2019.